

# Energetic Comparison between Photoinduced Electron-Transfer Reactions from NADH Model Compounds to Organic and Inorganic Oxidants and Hydride-Transfer Reactions from NADH Model Compounds to *p*-Benzoquinone Derivatives

Shunichi Fukuzumi, Shintaro Koumitsu, Katsuhiko Hironaka, and Toshio Tanaka\*

Contribution from the Department of Applied Chemistry, Faculty of Engineering, Osaka University, Suita, Osaka 565, Japan. Received November 5, 1985

**Abstract:** Kinetic studies on photoinduced electron-transfer reactions from dihydropyridine compounds (PyH<sub>2</sub>) as being NADH model compounds to organic and inorganic oxidants and hydride-transfer reactions from PyH<sub>2</sub> to *p*-benzoquinone derivatives (Q) in the absence and presence of Mg<sup>2+</sup> ion are reported by determining over 150 rate constants. These results, combined with the values of Gibbs energy change of the photoinduced electron-transfer reactions as well as those of each step of the hydride-transfer reactions as being the e<sup>-</sup>-H<sup>+</sup>-e<sup>-</sup> sequence, which are determined independently, revealed that the rate constants of the photoinduced electron-transfer reactions obey the Rehm-Weller-Gibbs energy relationship and that the activation barrier of the hydride-transfer reactions from PyH<sub>2</sub> to Q is dependent solely on the Gibbs energy changes of the initial electron transfer from PyH<sub>2</sub> to Q and the following proton transfer from PyH<sub>2</sub><sup>•+</sup> to Q<sup>-</sup> and thus independent of the Gibbs energy change of the final electron transfer from PyH<sup>•</sup> to QH<sup>•</sup>. The retarding effect of Mg<sup>2+</sup> ion observed on the photoinduced electron transfer and hydride-transfer reactions of PyH<sub>2</sub> is ascribed to the positive shifts of the redox potentials of the ground and excited states of PyH<sub>2</sub> due to the complex formation with Mg<sup>2+</sup> ion.

Many redox reactions that had been viewed simply as direct transfer of a two-electron equivalent such as a hydride ion or electrophile-nucleophile binding have recently been reconsidered as proceeding via one-electron transfer in the activation process, followed by the reaction in a resulting radical ion pair.<sup>1-4</sup> Since in many cases, the products and kinetics are the same regardless of the mechanisms, it seems to be difficult to distinguish between

these two mechanisms, often creating mechanistic controversies,<sup>5</sup> although in some cases detection of radical intermediates or isolation of products that could have arisen only via radicals represents good evidence for the electron-transfer mechanisms.<sup>4</sup> Especially, mechanisms of hydride-transfer reactions from reduced nicotinamide adenine dinucleoside (NADH) or its model compounds to substrates have been the subject of considerable controversy whether a hydride transfer occurs in a one-step<sup>6-13</sup> or consists of overall transfer of two electrons and a proton in a e<sup>-</sup>-H<sup>+</sup>-e<sup>-</sup> sequence.<sup>14-19</sup> However, such mechanistic distinction

(1) (a) Everson, L. *Adv. Phys. Org. Chem.* **1982**, *18*, 79. (b) Chanon, M. *Bull. Soc. Chim. Fr.* **1982**, II-197. (c) Julliard, N.; Chanon, M. *Chem. Rev.* **1983**, *83*, 425. (d) Chanon, M.; Tobe, M. L. *Angew. Chem., Int. Ed. Engl.* **1982**, *21*, 1. (e) House, H. O. *Acc. Chem. Res.* **1976**, *9*, 59. (f) Klingler, R. J.; Fukuzumi, S.; Kochi, J. K. *ACS Symp. Ser.* **1983**, *211*, 117.

(2) (a) Fukuzumi, S.; Wong, C. L.; Kochi, J. K. *J. Am. Chem. Soc.* **1980**, *102*, 2928. (b) Fukuzumi, S.; Mochida, K.; Kochi, J. K. *Ibid.* **1979**, *101*, 5961. (c) Fukuzumi, S.; Kochi, J. K. *Ibid.* **1980**, *102*, 2141, 7290. (d) Fukuzumi, S.; Kochi, J. K. *Ibid.* **1981**, *103*, 2783, 7240. (e) Fukuzumi, S.; Kochi, J. K. *Ibid.* **1982**, *104*, 7599. (f) Fukuzumi, S.; Kochi, J. K. *Tetrahedron.* **1982**, *38*, 1035. (g) Fukuzumi, S.; Kochi, J. K. *Bull. Chem. Soc. Jpn.* **1983**, *56*, 969. (h) Fukuzumi, S.; Nishizawa, N.; Tanaka, T. *Ibid.* **1982**, *55*, 2886. (i) Fukuzumi, S.; Nishizawa, N.; Tanaka, T. *Ibid.* **1983**, *56*, 709. (j) Fukuzumi, S.; Hironaka, K.; Tanaka, T. *J. Am. Chem. Soc.* **1983**, *105*, 4722. (k) Fukuzumi, S.; Kuroda, S.; Tanaka, T. *Ibid.* **1985**, *107*, 3020.

(3) (a) Ashby, E. C.; Goel, A. B. *J. Am. Chem. Soc.* **1981**, *103*, 4983. (b) Ashby, E. C.; Argyropoulos, J. N.; Meyer, G. R.; Goel, A. B. *Ibid.* **1982**, *104*, 6788. (c) Ashby, E. C.; Goel, A. B.; DePriest, R. N. *Ibid.* **1980**, *102*, 7779. (d) Wang, S. S.; Sucknik, C. N. *J. Org. Chem.* **1985**, *50*, 653. (e) Tamblin, W. H.; Vogler, E. A.; Kochi, J. K. *J. Org. Chem.* **1980**, *45*, 3912. (f) Klingler, R. J.; Mochida, K.; Kochi, J. K. *J. Am. Chem. Soc.* **1979**, *101*, 6626. (g) Tanner, D. D.; Blackburn, E. V.; Diaz, G. E. *Ibid.* **1981**, *103*, 1557. (h) Tanner, D. D.; Diaz, G. E.; Potter, A. J. *Org. Chem.* **1985**, *50*, 2149. (i) Pryor, W. A.; Hendrickson, W. H., Jr. *J. Am. Chem. Soc.* **1983**, *105*, 7114. (j) Zupancic, J. J.; Horn, K. A.; Schuster, G. B. *Ibid.* **1980**, *102*, 5279. (k) Lau, W.; Kochi, J. K. *Ibid.* **1984**, *106*, 7100.

(4) (a) Liotta, D.; Saindane, M.; Waykole, L. *J. Am. Chem. Soc.* **1983**, *105*, 2922. (b) Mattes, S. L.; Farid, S. *Ibid.* **1982**, *104*, 1454. (c) Ashby, E. C.; Bowers, J. R., Jr. *Ibid.* **1981**, *103*, 2242. (d) Ashby, E. C.; Su, W.-Y.; Pham, T. N. *Organometallics* **1985**, *4*, 1493. (e) Ashby, E. C.; DePriest, R. N.; Pham, T. N. *Tetrahedron Lett.* **1983**, *24*, 2825. (f) Hendrickson, W. H., Jr.; MacDonald, W. D.; Howard, S. T.; Coligado, E. J. *Ibid.* **1985**, *26*, 2939. (g) Newcomb, M.; Williams, W. G. *Ibid.* **1984**, *25*, 2723. (h) Ashby, E. C.; Goel, A. B.; DePriest, R. N. *J. Org. Chem.* **1981**, *46*, 2429. (i) Chung, S.-K.; Filmore, K. L. *J. Chem. Soc., Chem. Commun.* **1983**, 358. (j) Fukuzumi, S.; Kochi, J. K. *J. Org. Chem.* **1980**, *45*, 2654. (k) Eriksen, J.; Foote, C. S. *J. Am. Chem. Soc.* **1980**, *102*, 6083. (l) Novak, M.; Bruice, T. C. *Ibid.* **1977**, *99*, 8079. (m) Garst, J. F.; Smith, C. D. *Ibid.* **1976**, *98*, 1520. (n) Roberts, J. F., Jr.; Sugimoto, H.; Barrette, W. C., Jr.; Sawyer, D. T. *Ibid.* **1985**, *107*, 4556. (o) Smith, G. F.; Kuivila, H. G.; Simon, R.; Sultan, L. *Ibid.* **1981**, *103*, 833. (p) Ferguson, G.; Parvez, M.; Monaghan, P. K.; Puddephatt, R. J. *J. Chem. Soc., Chem. Commun.* **1983**, 267.

(5) (a) Perrin, C. L. *J. Phys. Chem.* **1984**, *88*, 3611. (b) Newcomb, M.; Burchill, M. T. *J. Am. Chem. Soc.* **1984**, *106*, 8276. (c) Hirabe, T.; Takagi, M.; Muraoka, K.; Nojima, M.; Kusabayashi, S. *J. Org. Chem.* **1985**, *50*, 1797. (d) Walling, C. *J. Am. Chem. Soc.* **1980**, *102*, 6854. (e) Scandola, F.; Balzani, V.; Schuster, G. B. *Ibid.* **1981**, *103*, 2519. (f) Walling, C.; Zhao, C. *Tetrahedron* **1982**, *38*, 1105. (g) Peacock, N. J.; Schuster, G. B. *J. Am. Chem. Soc.* **1983**, *105*, 3632.

(6) (a) Abeles, R. H.; Hutton, R. F.; Westheimer, F. H. *J. Am. Chem. Soc.* **1957**, *79*, 712. (b) Dittmer, D. C.; Fouty, R. A. *Ibid.* **1964**, *86*, 91. (c) Brüstlein, M.; Bruice, T. C. *Ibid.* **1972**, *94*, 6548.

(7) (a) Bunting, J. W.; Sindhuatmadja, S. *J. Org. Chem.* **1981**, *46*, 4211. (b) Bunting, J. W.; Chew, V. S. F.; Chu, G. *Ibid.* **1982**, *47*, 2303.

(8) (a) Stewart, R.; Norris, D. J. *J. Chem. Soc., Perkin Trans. 2* **1978**, 246. (b) Srinivasan, R.; Medary, R. T.; Fisher, H. F.; Norris, D. J.; Stewart, R. *J. Am. Chem. Soc.* **1982**, *104*, 807.

(9) (a) Powell, M. F.; Bruice, T. C. *J. Am. Chem. Soc.* **1983**, *105*, 1014, 7139. (b) Chipman, D. M.; Yaniv, R.; van Eikeren, P. *Ibid.* **1980**, *102*, 3244. (c) van Laar, A.; van Ramesdonk, H. J.; Verhoeven, J. W. *Recl. Trav. Chim. Pays-Bas* **1983**, *102*, 157.

(10) (a) Chung, S.-K.; Park, S.-U. *J. Org. Chem.* **1982**, *47*, 3197. (b) MacInnes, I.; Nonhebel, D. C.; Orszulik, S. T.; Suckling, C. J. *J. Chem. Soc., Perkin Trans. 1* **1983**, 2777. (c) van Nield, J. C. G.; Pandit, U. K. *J. Chem. Soc., Chem. Commun.* **1983**, 149. (d) MacInnes, I.; Nonhebel, D. C.; Orszulik, S. T.; Suckling, C. J. *Ibid.* **1982**, 121.

(11) (a) Roberts, R. M. G.; Ostovič, D.; Kreevoy, M. M. *Faraday Discuss. Chem. Soc.* **1982**, *74*, 257. (b) Ostovič, D.; Roberts, R. M. G.; Kreevoy, M. M. *J. Am. Chem. Soc.* **1983**, *105*, 7629. (c) Kreevoy, M. M.; Lee, I.-S. H. *Ibid.* **1984**, *106*, 2550.

(12) Donkersloot, M. C. A.; Buck, H. M. *J. Am. Chem. Soc.* **1981**, *103*, 6549, 6554.

(13) Kurtz, L. C.; Frieden, C. *J. Am. Chem. Soc.* **1975**, *97*, 677. Kurtz, L. C.; Frieden, C. *J. Am. Chem. Soc.* **1980**, *102*, 4198. Kurtz, L. C.; Frieden, C. *Biochemistry* **1977**, *16*, 5207.

(14) (a) Steffens, J. J.; Chipman, D. M. *J. Am. Chem. Soc.* **1971**, *93*, 6694. (b) Creighton, D. J.; Hajdu, J.; Mooser, G.; Sigman, D. S. *Ibid.* **1973**, *95*, 6855. (c) Sigman, D. S.; Hajdu, J.; Creighton, D. J. In *Bioorganic Chemistry*; van Tamelen, E. E., Ed.; Academic Press: New York, 1978; Vol. IV, p 385.

seems to be actually dubious and possibly even meaningless unless either mechanism provides a more quantitative description of the energetic profiles of the reactions than the other does.

We have previously reported a quantitative approach to delineate the energetic profiles of hydride-transfer reactions from an NADH model compound, 1-benzyl-1,4-dihydropyridinamide (BNAH), to a series of *p*-benzoquinone derivatives (Q) in the absence and presence of  $Mg^{2+}$  ion in acetonitrile (MeCN) as proceeding via  $e^-H^+-e^-$  sequence by showing that the rate constants and the primary kinetic isotope effects can be successfully correlated with the Gibbs energy change of the electron transfer from BNAH to Q.<sup>20,21</sup> Such a hydride transfer reaction via  $e^-H^+-e^-$  sequence proceeds in the pair and should be distinguished from an electron-transfer reaction when the pair separates to yield free radical ion,  $BNAH^{+\bullet}$  and  $Q^{\bullet-}$ .

Recently, Miller et al.<sup>22</sup> have reported an alternative elegant approach to describe the energetic profile of hydride-transfer reactions from NADH to Q in  $H_2O$  as proceeding by one-step hydride transfer by showing that the rate constants are related with the two-electron redox potentials for the  $Q/QH^-$  couple with a slope of 16.9  $V^{-1}$  and ruled out an electron-transfer mechanism based on the comparison of data with the one-electron-transfer reactions from NADH to ferricenium ions ( $Fc^+$ ) by assuming implicitly that the work terms  $w_p$  which are required to bring the product ions to the mean separation in the activated complex are the same between the  $NADH-Q$  and  $NADH-Fc^+$  systems.<sup>22,23</sup> However, the work term  $w_p$  of the radical ion pair [ $BNAH^{+\bullet} Q^{\bullet-}$ ] in MeCN which consists of the opposite charges could be largely negative and thereby quite different from  $w_p$  of the radical pair [ $NADH^{+\bullet} Fc$ ] in  $H_2O$  which contains a neutral species  $Fc$ . The importance of the work term  $w_p$  in electron-transfer processes has been pointed out,<sup>24</sup> especially in the case of those via charge-transfer (CT) complexes formed between neutral donor and acceptor molecules.<sup>2</sup> In fact, the CT complexes formed between an NADH model compound and *p*-benzoquinone derivatives have been isolated, and the transient CT spectra have been detected during the hydride-transfer reactions from BNAH to Q.<sup>20</sup>

We report here the systematic kinetic studies on electron-transfer reactions from NADH model compounds to the excited states of  $[RuL_3]^{2+}$  and  $[RuL_2L']$  ( $L = 2,2'$ -bipyridine and  $L' = 4,4'$ -(COO<sup>-</sup>)<sub>2</sub>bpy) which have different charges and those from the excited states of BNAH to various neutral organic oxidants by considering the difference of the work term  $w_p$  as well as on hydride-transfer reactions from various NADH model compounds to *p*-benzoquinone derivatives by determining independently the

energetics of each step of the hydride-transfer reactions, i.e., the Gibbs energy changes of the  $e^-H^+-e^-$  sequence. We wish to compare the two approaches to describe the energetic profiles of the hydride-transfer reactions; one is the correlation of the rate constants for both the photoinduced electron-transfer and hydride-transfer reactions with the Gibbs energy change of the electron transfer  $\Delta G^\circ_{et}$ , and the other is the correlation of the rate constants of the hydride-transfer reactions with the Gibbs energy change of the overall transfer of a hydride ion  $\Delta G^\circ_H$  which is equal to the sum of the Gibbs energy changes of the  $e^-H^+-e^-$  sequence. Different types of dihydropyridine ( $PyH_2$ ) such as 1-(substituted benzyl)-1,4-dihydropyridinamide ( $X-BNAH$ ) and *N*-methylacridin ( $AcH_2$ ) which have similar one-electron redox potentials  $E^\circ(PyH_2^{+\bullet}/PyH_2)$  but different two-electron redox potentials  $E^\circ(PyH^+/PyH_2)$  are chosen as NADH model compounds so that it can be determined which factor ( $\Delta G^\circ_{et}$  or  $\Delta G^\circ_H$ ) reflects the change of the activation barrier of the hydride-transfer reactions better. *p*-Benzoquinone derivatives may be the best choice as the substrates for the purpose of this study since the thermodynamic data concerning the quinone-hydroquinone systems are well characterized.<sup>25</sup> We report also the role of  $Mg^{2+}$  ion on both the photoinduced electron-transfer and hydride-transfer reactions of NADH model compounds.

## Experimental Section

**Materials.** Dihydropyridine derivatives, 1-benzyl-1,4-dihydropyridinamide (BNAH),<sup>26</sup> 1-(*X*-benzyl)-1,4-dihydropyridinamides (*X*-BNAH:  $X = 4-MeO, 4-Me, 4-Cl,$  and  $2,4-Cl_2$ ),<sup>26,27</sup> 2,6-dimethyl-3,5-dicarbethoxy-1,4-dihydropyridine (Hantzsch's ester),<sup>28</sup> 1-benzyl-3-carbamoyl-1,4-dihydroquinoline (BCQH),<sup>29</sup> and *N*-methylacridin ( $AcH_2$ )<sup>11</sup> were prepared according to the literatures. All the pyridinium cations ( $PyH^+$ ) which are the oxidized forms of dihydropyridine derivatives were obtained as the perchlorate salts by the addition of magnesium perchlorate to the halide salts in water. The elemental analyses of all the dihydropyridine derivatives gave satisfactory results. Tris(2,2'-bipyridine)ruthenium(II) dichloride hexahydrate  $[RuL_3]Cl_2 \cdot 6H_2O$ ,<sup>30</sup> bis(2,2'-bipyridine)-4,4'-dicarbethoxy-2,2'-bipyridineruthenium(II) hexafluorophosphate, which dissociates to give  $[RuL_2L']$  ( $L' = 4,4'$ -(COO<sup>-</sup>)<sub>2</sub>bpy) in MeCN,<sup>31</sup> and tris(2,2'-bipyridine)iron(III) perchlorate  $[FeL_3](ClO_4)_3$ <sup>32</sup> were prepared according to the literatures. Organic oxidants (*N,N*-dimethylaniline, *N,N*-dimethyl-*p*-toluidine, *N,N'*-diphenyl-*p*-phenylenediamine) and oxidants (1-cyanonaphthalene, *trans*-stilbene, and cyanobenzene) used as quenchers for the luminescence quenching of  $[RuL_3]^{2+}$  and  $[RuL_2L']$  were obtained commercially and purified by the standard method.<sup>32</sup> Most *p*-benzoquinone derivatives (2,3-dichloro-5,6-dicyano-*p*-benzoquinone, *p*-chloranil, *p*-bromanil, 2,6-dichloro-*p*-benzoquinone, *p*-benzoquinone, methyl-*p*-benzoquinone, and 2,6-dimethyl-*p*-benzoquinone) were also obtained commercially and purified by the standard methods.<sup>32</sup> Chloro-*p*-benzoquinone and 2,3-dicyano-*p*-benzoquinone were prepared from the corresponding hydroquinones according to the literature.<sup>33</sup> Anhydrous magnesium perchlorate was obtained from Nakarai Chemicals. Acetonitrile which was also obtained commercially was purified and dried with calcium hydride by the standard procedure<sup>32</sup> and stored under nitrogen atmosphere.

**Luminescence Quenching.** Quenching experiments of the BNAH fluorescence and the  $[RuL_3]^{2+}$  and  $[RuL_2L']$  luminescence were performed by using a Hitachi 650-10S fluorescence spectrophotometer. The excitation wavelengths were 350, 363, 452, and 470 nm for BNAH in the absence of  $Mg^{2+}$  ion, BNAH in the presence of  $Mg^{2+}$  ion, and  $[RuL_3]^{2+}$  and  $[RuL_2L']$  in MeCN, respectively. The monitoring wave-

- (15) (a) Ohno, A.; Yamamoto, H.; Oka, S. *J. Am. Chem. Soc.* **1981**, *103*, 2041. (b) Ohno, A.; Shio, T.; Yamamoto, H.; Oka, S. *Ibid.* **1981**, *103*, 2045. (c) Ohno, A.; Nakai, J.; Nakamura, K.; Goto, T.; Oka, S. *Bull. Chem. Soc. Jpn.* **1981**, *54*, 3486. (d) Yasui, S.; Nakamura, K.; Ohno, A.; Oka, S. *Ibid.* **1982**, *55*, 196. (e) Ohno, A.; Kobayashi, H.; Goto, T.; Oka, S. *Ibid.* **1984**, *57*, 1279. (f) Ohno, A.; Kobayashi, H.; Oka, S.; Goto, T. *Tetrahedron Lett.* **1983**, *24*, 5123. (g) Ohno, A.; Kobayashi, H.; Nakamura, K.; Oka, S. *Ibid.* **1983**, *24*, 1263. (h) Yasui, S.; Nakamura, K.; Ohno, A. *Ibid.* **1983**, *24*, 3331. (i) Bunting, J. W.; Chew, V. S. F.; Chu, G.; Fitzgerald, N. P.; Gunasekara, A.; Oh, H. T. P. *Bioorg. Chem.* **1984**, *12*, 141.
- (16) (a) Shinkai, S.; Tsuno, T.; Asatani, Y.; Manabe, O. *J. Chem. Soc., Perkin Trans. 2* **1983**, 1533. (b) Shinkai, S.; Ide, T.; Hamada, H.; Manabe, O.; Kunitake, T. *J. Chem. Soc., Chem. Commun.* **1977**, 848. (c) Shinkai, S.; Tsuno, T.; Manabe, O. *Ibid.* **1982**, 592. (d) Shinkai, S.; Tsuno, T.; Manabe, O. *Chem. Lett.* **1981**, 1203.
- (17) (a) Fukuzumi, S.; Kondo, Y.; Tanaka, T. *J. Chem. Soc., Perkin Trans. 2* **1984**, 673. (b) Fukuzumi, S.; Kondo, Y.; Tanaka, T. *Chem. Lett.* **1982**, 1591. (c) Fukuzumi, S.; Kondo, Y.; Tanaka, T. *Ibid.* **1983**, 751.
- (18) (a) Lai, C. C.; Colter, A. K. *J. Chem. Soc., Chem. Commun.* **1980**, 1115. (b) Jarvis, W. F.; Dittmer, D. C. *J. Org. Chem.* **1983**, *48*, 2784.
- (19) (a) van Eikeren, P.; Kenney, P.; Tokmakian, R. *J. Am. Chem. Soc.* **1979**, *101*, 7402. (b) van Eikeren, P.; Grier, D. L.; Eliason, J. *Ibid.* **1979**, *101*, 7406.
- (20) (a) Fukuzumi, S.; Nishizawa, N.; Tanaka, T. *J. Org. Chem.* **1984**, *49*, 3571. (b) Fukuzumi, S.; Tanaka, T. *Chem. Lett.* **1982**, 1513.
- (21) (a) Fukuzumi, S.; Nishizawa, N.; Tanaka, T. *J. Chem. Soc., Perkin Trans. 2* **1985**, 371. (b) Fukuzumi, S.; Nishizawa, N.; Tanaka, T. *Chem. Lett.* **1983**, 1755.
- (22) Carlson, B. W.; Miller, L. L. *J. Am. Chem. Soc.* **1985**, *107*, 479.
- (23) Verhoeven, J. W.; van Gerresheim, W.; Martens, F. M.; van der Kerk, S. M. *Tetrahedron* **1986**, *42*, 975.
- (24) Haim, A.; Sutin, N. *Inorg. Chem.* **1976**, *15*, 476.

- (25) (a) Rich, P. R.; Bendall, D. S. *Biochim. Biophys. Acta* **1980**, *592*, 506. (b) Patel, K. B.; Willson, R. L. *J. Chem. Soc., Faraday Trans. 1* **1973**, 814. (c) Meisel, D.; Czapski, G. *J. Phys. Chem.* **1975**, *79*, 1503. (d) Pelizzetti, E.; Mentasti, E.; Baiocchi, C. *Ibid.* **1976**, *80*, 2979.
- (26) Mauserall, D.; Westheimer, F. H. *J. Am. Chem. Soc.* **1955**, *77*, 2261.
- (27) Bunting, J. W.; Sindhuatmaja, S. *J. Org. Chem.* **1981**, *46*, 4219.
- (28) Meyer, H.; Tropsch, H. *Monaish.* **1914**, *35*, 207.
- (29) (a) Munshi, J. F.; Joulie, M. M. *Tetrahedron* **1968**, *24*, 1923. (b) Shinkai, S.; Hamada, H.; Kusana, Y.; Manabe, O. *J. Chem. Soc., Perkin Trans. 2* **1979**, 699.
- (30) Burstall, F. H. *J. Chem. Soc.* **1936**, 173.
- (31) (a) Sprintschnik, G.; Sprintschnik, H. W.; Kirsch, P. P.; Whitten, D. G. *J. Am. Chem. Soc.* **1977**, *99*, 4947. (b) Cherry, W. R.; Henderson, L. J. Jr., *Inorg. Chem.* **1984**, *23*, 983.
- (32) Perrin, D. D.; Armarego, W. L. F.; Perrin, D. R. *Purification of Laboratory Chemicals*; Pergamon Press: New York, 1966.
- (33) (a) Cason, J.; Allen, C. F.; Goodwin, G. *J. Org. Chem.* **1948**, *13*, 403. (b) Brook, A. G. *J. Chem. Soc.* **1953**, 5040.

lengths were those corresponding to the maxima of the respective emission bands at 443, 455, 608, and 630 nm. Relative emission intensities were measured for MeCN solutions of BNAH,  $[\text{RuL}_3]^{2+}$ , and  $[\text{RuL}_2\text{L}']$  containing  $n\text{-Bu}_4\text{NClO}_4$  ( $1.0 \times 10^{-2}$  or  $0.10$  M) with a quencher at various concentrations. The solutions of  $[\text{RuL}_3]^{2+}$  and  $[\text{RuL}_2\text{L}']$  were degassed and replaced by an atmospheric pressure of nitrogen prior to the measurements. There has been no change in the shape except intensity of the emission spectrum by the addition of a quencher. The Stern-Volmer relationship (eq 1) was obtained between the ratio of the

$$I_f^0/I_f = 1 + K_q[q] \quad (1)$$

emission intensities in the absence and presence of a quencher  $I_f^0/I_f$  and the quencher concentration  $[q]$ . The observed rate constant  $k_{\text{obsd}} (= K_q\tau^{-1})$  was determined from the Stern-Volmer constants  $K_q$  and the emission lifetime  $\tau$  (BNAH 0.76 ns,<sup>34</sup> BNAH in the presence of  $\text{Mg}^{2+}$  ion 1.03 ns,<sup>35</sup>  $[\text{RuL}_3]^{2+}$  850 ns,<sup>36</sup> and  $[\text{RuL}_2\text{L}']$  850 ns<sup>36</sup>).

**Cyclic Voltammetry.** Reduction potentials of  $[\text{RuL}_2\text{L}']$  and organic oxidants which have not been reported were determined by the cyclic voltammetry measurements, which were performed on a Hokuto Denko Model HA-301 potentiostat-galvanostat at 298 K in MeCN containing 0.10 M  $n\text{-Bu}_4\text{NClO}_4$  as a supporting electrolyte by using a saturated calomel electrode (SCE) or an Ag/Ag<sup>+</sup> electrode (Ag/AgNO<sub>3</sub> 0.10 M) as a reference one under deaerated conditions; the redox potential vs. Ag/Ag<sup>+</sup> is more negative by 0.34 V than that vs. SCE.<sup>37</sup> The one-electron redox potentials of  $\text{PyH}_2$   $E^\circ(\text{PyH}_2^{+}/\text{PyH}_2)$  and  $\text{PyH}^+$   $E^\circ(\text{PyH}^+/\text{PyH}^*)$  in the absence and presence of  $\text{Mg}^{2+}$  ion were determined by analyzing the cyclic voltammograms at various sweep rates in the range 10–1000 mV s<sup>-1</sup>, based on the method described in detail elsewhere.<sup>21,38</sup> The platinum microelectrode was routinely cleaned by soaking it in concentrated nitric acid, followed by repeating rinsing with water and acetone, and drying at 353 K prior to use. The anodic and cathodic peak potentials of  $\text{PyH}_2$   $E_{\text{ox}}^p$  and  $\text{PyH}^+$   $E_{\text{red}}^p$ , respectively, were reproducible to within  $\pm 20$  mV at a constant sweep rate. Little deterioration of the electrode was observed upon repeated scans, indicating that anodic oxidation of  $\text{PyH}_2$  or cathodic reduction of  $\text{PyH}^+$  leads to products without fouling of the electrode surface.

**Kinetic Measurements.** Kinetic measurements were performed under deaerated conditions by using a Union RA-103 stopped flow spectrophotometer and a Union SM-401 spectrophotometer for fast reactions of  $\text{PyH}_2$  with  $[\text{Fe}(\text{bpy})_3]^{3+}$  and  $p$ -benzoquinone derivatives (Q) with half-lives shorter than 10 s and for the slower reactions of  $\text{PyH}_2$  with Q with half-lives much longer than 10 s, respectively. Rates of the electron-transfer reactions from  $\text{PyH}_2$  to  $[\text{Fe}(\text{bpy})_3]^{3+}$  in MeCN containing an excess amount of pyridine derivative to  $\text{PyH}_2$  were followed by the increase in absorbance at  $\lambda_{\text{max}} = 507$  nm due to  $[\text{Fe}(\text{bpy})_3]^{2+}$ .<sup>39</sup> Rates of the hydride-transfer reactions from X-BNAH to Q in the absence and presence of  $\text{Mg}^{2+}$  ion in MeCN at 298 K were determined by the increase in absorbance at the absorption maxima of the respective semiquinone radical anions<sup>20</sup> and by the decrease in absorbance at  $\lambda_{\text{max}}$  of X-BNAH, respectively. Rates of the hydride-transfer reactions from AcH<sub>2</sub> to Q in both the absence and presence of  $\text{Mg}^{2+}$  ion in MeCN at 298 K were monitored by the increase in absorbance due to AcH<sup>+</sup> in the visible region ( $\lambda_{\text{max}} 358$  nm,  $\epsilon 2.00 \times 10^4$  M<sup>-1</sup> cm<sup>-1</sup>). All the kinetic measurements were carried out under the pseudo-first-order conditions by using more than 10-fold excess substrates. Especially, in the case of the hydride-transfer reaction from AcH<sub>2</sub> to chloro- $p$ -benzoquinone in the absence of  $\text{Mg}^{2+}$  ion in MeCN at 298 K, more than 500-fold excess of the quinone was used in order to neglect the back reaction. The pseudo-first-order rate constants were determined by the least-square curve fit, by using a Union System 77 microcomputer.

## Results

### Photoinduced Electron-Transfer Reactions of NADH Model Compounds.

The luminescence of  $[\text{RuL}_3]^{2+}$  ( $\lambda_{\text{max}} 608$  nm,  $\tau 850$  ns)

(34) Martens, F. M.; Verhoeven, J. W.; Gase, R. A.; Pandit, U. K.; de Bore, Th. J. *Tetrahedron* **1978**, *34*, 443.

(35) The fluorescence lifetime  $\tau$  of BNAH\* in the presence of  $\text{Mg}^{2+}$  ion is estimated from the  $K_q$  value for diethyl fumarate, which is assumed to be diffusion limited ( $k_{\text{diff}} = 2.0 \times 10^{10}$  M<sup>-1</sup> s<sup>-1</sup>).

(36) (a) Boch, C. R.; Conner, J. A.; Gutierrez, A. R.; Meyer, T. J.; Whitten, D. G.; Sullivan, B. P.; Nagle, J. K. *J. Am. Chem. Soc.* **1979**, *101*, 4815. (b) The luminescence lifetime  $\tau$  of  $[\text{RuL}_2\text{L}']^*$  in MeCN is taken to be the same as that of  $[\text{RuL}_3]^{2+}$  in MeCN since their  $\tau$  values in D<sub>2</sub>O are identical (ref 31b).

(37) Mann, C. K. *Electroanal. Chem.* **1969**, *4*, 57.

(38) Fukuzumi, S.; Hironaka, K.; Nishizawa, N.; Tanaka, T. *Bull. Chem. Soc. Jpn.* **1983**, *56*, 2220.

(39) Fukuzumi, S.; Nishizawa, N.; Tanaka, T. *Bull. Chem. Soc. Jpn.* **1982**, *55*, 3482.

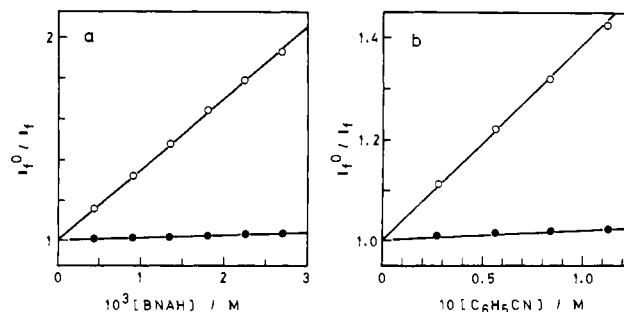


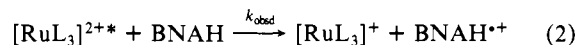
**Figure 1.** Stern-Volmer plots (a) for the luminescence quenching of  $[\text{RuL}_3]^{2+*}$  ( $1.3 \times 10^{-5}$  M) by BNAH in the absence (O) and presence of  $1.0 \times 10^{-2}$  M  $\text{Mg}(\text{ClO}_4)_2$  (●) in MeCN containing  $1.0 \times 10^{-2}$  M  $n\text{-Bu}_4\text{NClO}_4$  and (b) for the fluorescence quenching of BNAH\* ( $1.8 \times 10^{-4}$  M) by cyanobenzene in the absence (O) and presence of  $5.0 \times 10^{-2}$  M  $\text{Mg}(\text{ClO}_4)_2$  (●) in MeCN at 298 K.

**Table I.** Rate Constants  $k_{\text{obsd}}$  for the Luminescence Quenching of  $[\text{RuL}_3]^{2+*}$  and  $[\text{RuL}_2\text{L}']^*$  by Organic Reductants ( $\text{PyH}_2$  and Aromatic Amines) in MeCN at 298 K

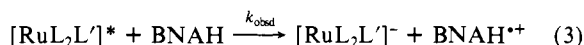
reductant	$k_{\text{obsd}}$ (M <sup>-1</sup> s <sup>-1</sup> ) <sup>a</sup> in the presence of $1.0 \times 10^{-2}$ M			
	$[\text{RuL}_3]^{2+*}$ $n\text{-Bu}_4\text{NClO}_4$	$[\text{RuL}_3]^{2+*}$ $\text{NaClO}_4$	$[\text{RuL}_3]^{2+*}$ $\text{Mg}(\text{ClO}_4)_2$	$[\text{RuL}_2\text{L}']^*$ $n\text{-Bu}_4\text{NClO}_4$
4-MeOBNAH	$8.5 \times 10^8$	$7.3 \times 10^8$	$8.6 \times 10^7$	$2.6 \times 10^9$
4-MeBNAH	$5.5 \times 10^8$	$5.5 \times 10^8$	$8.6 \times 10^7$	$1.7 \times 10^9$
BNAH	$4.1 \times 10^8$	$3.8 \times 10^8$	$1.5 \times 10^7$	$1.1 \times 10^9$
4-ClBNAH	$2.8 \times 10^8$	$2.7 \times 10^8$	$1.2 \times 10^7$	$6.8 \times 10^8$
2,4-Cl <sub>2</sub> BNAH	$2.1 \times 10^8$	$1.7 \times 10^8$	$1.2 \times 10^7$	$6.0 \times 10^8$
Hantzsch's ester	$1.2 \times 10^8$	$1.1 \times 10^8$	$<10^6$	
BCQH	$6.3 \times 10^7$		$<10^6$	
<i>N,N</i> -dimethyl-aniline	$9.4 \times 10^7$ <sup>b</sup>	$8.5 \times 10^7$	$9.1 \times 10^7$	
<i>N,N</i> -dimethyl- <i>p</i> -toluidine	$9.4 \times 10^8$ <sup>b</sup>	$8.7 \times 10^8$	$8.8 \times 10^8$	
<i>N,N'</i> -diphenyl- <i>p</i> -phenylenediamine	$5.6 \times 10^9$ <sup>b</sup>	$5.7 \times 10^9$	$5.4 \times 10^9$	

<sup>a</sup> The experimental errors are within  $\pm 5\%$ . <sup>b</sup> Similar values are reported in ref 40.

ns) is known to be quenched by the electron-transfer reactions from various electron donors to  $[\text{RuL}_3]^{2+*}$ .<sup>36,40</sup> When the absorption band of  $[\text{RuL}_3]^{2+}$  in MeCN containing BNAH was excited at  $\lambda_{\text{max}} 452$  nm where BNAH has no absorption band, BNAH efficiently quenched the  $[\text{RuL}_3]^{2+*}$  luminescence by the electron transfer from BNAH to  $[\text{RuL}_3]^{2+*}$  (eq 2). The observed



rate constant  $k_{\text{obsd}}$  in a deaerated MeCN solution containing  $1.0 \times 10^{-2}$  M  $n\text{-Bu}_4\text{NClO}_4$  is determined as  $4.1 \times 10^8$  M<sup>-1</sup> s<sup>-1</sup> from the Stern-Volmer plot in Figure 1a. The  $k_{\text{obsd}}$  values for various NADH model compounds are listed in Table I. NADH model compounds quenched also the luminescence of  $[\text{RuL}_2\text{L}']^*$  ( $\lambda_{\text{max}} 630$  nm,  $\tau 850$  ns)<sup>36</sup> in MeCN containing  $1.0 \times 10^{-2}$  M  $n\text{-Bu}_4\text{NClO}_4$  by the electron-transfer reactions from NADH model compounds to  $[\text{RuL}_2\text{L}']^*$  (eq 3). The  $k_{\text{obsd}}$  values are also listed



in Table I, where the  $k_{\text{obsd}}$  values in both cases (eq 2 and 3) decrease with decreasing the donor ability of the substituent on BNAH.

When  $\text{Mg}(\text{ClO}_4)_2$  was added to the  $[\text{RuL}_3]^{2+*}$ -BNAH system,  $k_{\text{obsd}}$  value decreased remarkably with an increase of the  $\text{Mg}^{2+}$  concentration as shown in Figure 1a. A similar retarding effect of  $\text{Mg}^{2+}$  ion was observed in the reductive quenching of  $[\text{RuL}_3]^{2+*}$  by other NADH model compounds; the  $k_{\text{obsd}}$  values in the presence

(40) Ballardini, R.; Varani, G.; Indelli, M. T.; Scandola, F.; Balzani, V. *J. Am. Chem. Soc.* **1978**, *100*, 7219.

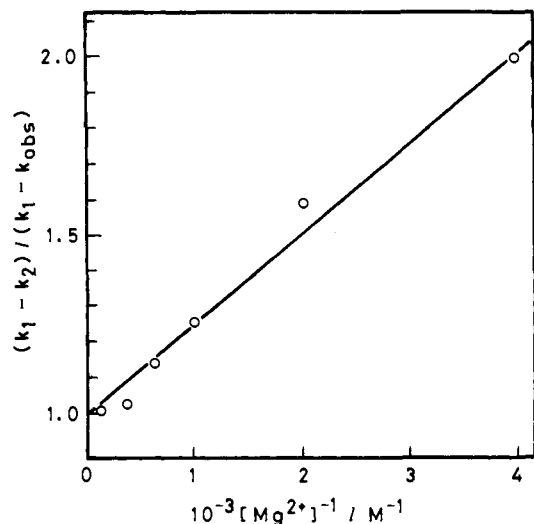
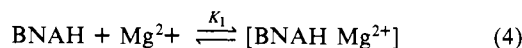


Figure 2. Plot of  $(k_1 - k_2)/(k_1 - k_{\text{obs}})$  vs.  $[\text{Mg}^{2+}]^{-1}$  for the luminescence quenching of  $[\text{RuL}_3]^{2+*}$  by the electron transfer from BNAH to  $[\text{RuL}_3]^{2+*}$  in the presence of  $\text{Mg}^{2+}$  ion in MeCN at 298 K.

of  $1.0 \times 10^{-2}$  M  $\text{Mg}^{2+}$  ion are shown in Table I. Such a retarding effect may be caused by the specific interaction of NADH model compounds with  $\text{Mg}^{2+}$  ion, since no effect of  $\text{Mg}^{2+}$  ion has been observed on the  $[\text{RuL}_3]^{2+*}$  luminescence quenching by aromatic amines (*N,N*-dimethylaniline, *N,N*-dimethyl-*p*-toluidine, and *N,N'*-diphenyl-*p*-phenylenediamine) as quenchers and no retarding effect has been detected in the presence of other metal ion ( $1.0 \times 10^{-2}$  M  $\text{NaClO}_4$ ) either (Table I). In fact, BNAH is known to form a 1:1 complex with  $\text{Mg}^{2+}$  ion (eq 4) with the formation



constant  $K_1 = 1.2 \times 10^4$  M $^{-1}$  in MeCN at 298 K.<sup>41</sup> In the presence of  $\text{Mg}^{2+}$  ion, the electron transfer from both BNAH and  $[\text{BNAH Mg}^{2+}]$  to  $[\text{RuL}_3]^{2+*}$  may occur, and then the observed rate constant  $k_{\text{obs}}$  in the presence of  $\text{Mg}^{2+}$  ion may be expressed by eq 5 where  $k_1$  and  $k_2$  are the rate constants in the absence of

$$k_{\text{obs}} = \frac{k_1 + k_2 K_1 [\text{Mg}^{2+}]}{1 + K_1 [\text{Mg}^{2+}]} \quad (5)$$

$\text{Mg}^{2+}$  ion and in the presence of a large excess  $\text{Mg}^{2+}$  ion such that all BNAH molecules form the 1:1 complex with  $\text{Mg}^{2+}$  ion, respectively. Equation 5 is rewritten by eq 6, the validity of which

$$\frac{(k_1 - k_2)}{(k_1 - k_{\text{obs}})} = 1 + \frac{1}{K_1 [\text{Mg}^{2+}]} \quad (6)$$

is shown by the linear plot of  $(k_1 - k_2)/(k_1 - k_{\text{obs}})$  vs.  $[\text{Mg}^{2+}]^{-1}$  in Figure 2. The  $K_1$  value which is obtained from the reciprocal of the slope in Figure 2 ( $K_1 = 3.6 \times 10^3$  M $^{-1}$ ) is somehow smaller than the value which was reported previously,<sup>41</sup> since the presence of water contained in  $[\text{RuL}_3]\text{Cl}_2 \cdot 6\text{H}_2\text{O}$  is known to decrease the  $K_1$  value in MeCN.<sup>41</sup> Thus, the observed rate constant  $k_{\text{obs}}$  in the presence of large excess  $\text{Mg}^{2+}$  ion corresponds to the rate constants for the electron transfer from  $[\text{BNAH Mg}^{2+}]$  to  $[\text{RuL}_3]^{2+*}$ .

The excitation of the absorption band ( $\lambda_{\text{max}}$  350 nm) of an MeCN solution of BNAH results in a fluorescence ( $\lambda_{\text{max}}$  443 nm,  $\tau$  0.76 ns).<sup>34</sup> The BNAH fluorescence is known to be quenched by the electron transfer from BNAH\* to organic oxidants (ox) in MeCN (eq 7).<sup>34,39</sup> A retarding effect of  $\text{Mg}^{2+}$  ion is observed



also in the oxidative quenching of BNAH\* by an organic oxidant in MeCN as shown in Figure 1b. The  $k_{\text{obs}}$  values for various organic oxidants in the absence and presence of  $5.0 \times 10^{-2}$  M  $\text{Mg}^{2+}$

Table II. Rate Constants  $k_{\text{obs}}$  for the Fluorescence Quenching of BNAH\* by Organic Oxidants in the Absence and Presence of  $\text{Mg}^{2+}$  Ion and Their One-Electron Reduction Potentials  $E^\circ(\text{ox}/\text{ox}^-)$  (vs. SCE) in MeCN

oxidant	$E^\circ(\text{ox}/\text{ox}^-)$ V	$k_{\text{obs}}$ (M $^{-1}$ s $^{-1}$ ) <sup>c</sup> at the $\text{Mg}^{2+}$ concentration (M)	
		0 <sup>d</sup>	$5.0 \times 10^{-2}$
diethyl fumarate	-1.50 <sup>a</sup>	$1.4 \times 10^{10}$	$2.0 \times 10^{10}$
diethyl terephthalate	-1.78 <sup>a</sup>	$1.7 \times 10^{10}$	
benzophenone	-1.86 <sup>a</sup>	$1.7 \times 10^{10}$	
1-cyanonaphthalene	-1.96 <sup>a</sup>	$1.6 \times 10^{10}$	$6.1 \times 10^9$
acetophenone	-2.10 <sup>a</sup>	$9.1 \times 10^9$	$8.1 \times 10^9$
propionophenone	-2.15 <sup>b</sup>	$9.1 \times 10^9$	
<i>trans</i> -stilbene	-2.20 <sup>a</sup>	$5.8 \times 10^9$	$8.1 \times 10^8$
4-methylacetophenone	-2.20 <sup>b</sup>	$6.7 \times 10^9$	$4.9 \times 10^9$
4-methoxyacetophenone	-2.22 <sup>b</sup>	$5.9 \times 10^9$	$4.1 \times 10^9$
cyanobenzene	-2.35 <sup>a</sup>	$4.9 \times 10^9$	$2.5 \times 10^8$
methyl benzoate	-2.37 <sup>a</sup>	$4.4 \times 10^9$	$7.4 \times 10^8$
ethyl benzoate	-2.40 <sup>a</sup>	$3.6 \times 10^9$	$1.4 \times 10^9$

<sup>a</sup> Taken from ref 34. <sup>b</sup> Determined by the cyclic voltammograms (see Experimental Section). <sup>c</sup> The experimental errors are within  $\pm 5\%$ . <sup>d</sup> Taken from ref 38.

ion are listed in Table II, together with the one-electron reduction potentials of organic oxidants. The  $k_{\text{obs}}$  value in the absence of  $\text{Mg}^{2+}$  ion increases with the positive shift of the one-electron reduction potentials of organic oxidants to reach the value close to diffusion limited. In the presence of  $5.0 \times 10^{-2}$  M  $\text{Mg}^{2+}$  ion, the  $k_{\text{obs}}$  values are smaller than those in its absence, except for the case of diethyl fumarate in which the rate constants in both the absence and presence of  $\text{Mg}^{2+}$  ion are close to diffusion limited as shown in Table II, where the retarding effect of  $\text{Mg}^{2+}$  ion is pronounced in the case of organic oxidants (1-cyanonaphthalene, *trans*-stilbene, and cyanobenzene) which have no carbonyl group to interact with  $\text{Mg}^{2+}$  ion.

**Redox Potentials of PyH<sub>2</sub> and PyH<sup>+</sup>.** The one-electron oxidation and reduction potentials of PyH<sub>2</sub>,  $E^\circ(\text{PyH}_2^{*+}/\text{PyH}_2)$  and PyH<sup>+</sup>,  $E^\circ(\text{PyH}^+/\text{PyH}^*)$ , respectively, in the absence and presence of  $\text{Mg}^{2+}$  ion in MeCN were determined by analyzing the cyclic voltammograms at various sweep rates, based on the method to determine the redox potentials in irreversible systems,<sup>21,38</sup> as follows. The cyclic voltammograms of PyH<sub>2</sub> in the absence and presence of  $\text{Mg}^{2+}$  ion are characterized by well-defined anodic waves, but no cathodic waves were observed on the reverse scan, even at high scan rates. Conversely, those of PyH<sup>+</sup> show well-defined cathodic waves but no corresponding anodic waves. The irreversible behavior suggests that the radical species formed on anodic oxidation or cathodic reduction is unstable and the follow-up chemical reaction is fast on the time scale of the CV measurements. Assuming that the follow-up chemical reaction is not rate-limiting, the width of the wave  $E^p - E^{p/2}$  in such an irreversible system has been shown to depend only on the transfer coefficient  $\beta$  according to eq 8<sup>1f,38,42</sup> where  $F$  is the Faraday

$$E^p - E^{p/2} = 1.857(RT/\beta F) \quad (8)$$

constant. It should be noted that not only  $E^p$  but also  $E^p - E^{p/2}$  varies with the sweep rate.<sup>42</sup> Thus, the transfer coefficient  $\beta$  defined by the tangent of the Gibbs energy change of electron transfer  $\partial \Delta G_{\text{et}}^* / \partial \Delta G_{\text{et}}^\circ$  at the peak potential is obtained from the width of the wave  $E^p - E^{p/2}$  by using eq 9, which is derived from eq 8. On the other hand, the activation Gibbs energy of electron

$$\beta = \frac{1.857RT}{F(E^p - E^{p/2})} \quad (9)$$

transfer  $\Delta G_{\text{et}}^*$  is expressed as a function of the standard Gibbs

(42) (a) Nicholson, R. S.; Shain, I. *Anal. Chem.* **1964**, *36*, 706. (b) Klingler, R. J.; Kochi, J. K. *J. Am. Chem. Soc.* **1980**, *102*, 4790. (c) Tamblyn, W. H.; Klingler, R. J.; Hwang, W. S.; Kochi, J. K. *Ibid.* **1981**, *103*, 3161. (d) Klingler, R. J.; Kochi, J. K. *Ibid.* **1982**, *104*, 4186. (e) Klingler, R. J.; Kochi, J. K. *Ibid.* **1981**, *103*, 5839. (f) Klingler, R. J.; Kochi, J. K. *J. Phys. Chem.* **1981**, *85*, 1731.

**Table III.** One-Electron Oxidation and Reduction Potentials (vs. SCE) of PyH<sub>2</sub> and PyH<sup>+</sup>, Respectively, in the Absence and Presence of Mg<sup>2+</sup> Ion in MeCN at 298 K<sup>a</sup>

PyH <sub>2</sub>	E°(PyH <sub>2</sub> <sup>•+</sup> /PyH <sub>2</sub> ) <sup>b</sup> V	E°(PyH <sub>2</sub> <sup>•+</sup> /PyH <sub>2</sub> ) <sup>c</sup> V
4-MeOBNAH	0.50	0.68
4-MeBNAH	0.54	0.70
BNAH	0.57	0.80
4-CIBNAH	0.62	0.77
2,4-Cl <sub>2</sub> BNAH	0.59	0.78
Hantzsch's ester	0.72	0.94
AcH <sub>2</sub>	0.80	0.79

PyH <sup>+</sup>	E°(PyH <sup>•+</sup> /PyH <sup>+</sup> ) <sup>b</sup> V
4-MeBNA <sup>•+</sup>	-1.13
BNA <sup>•+</sup>	-1.08
4-CIBNA <sup>•+</sup>	-1.08
2,4-Cl <sub>2</sub> BNA <sup>•+</sup>	-1.08
AcH <sup>•+</sup>	-0.43

<sup>a</sup> Determined by the analysis of the cyclic voltammograms (see text and ref 21 and 38). The experimental errors are within ±5%. <sup>b</sup> In the presence of 0.10 M *n*-Bu<sub>4</sub>NClO<sub>4</sub>. <sup>c</sup> In the presence of 5.0 × 10<sup>-2</sup> M Mg(ClO<sub>4</sub>)<sub>2</sub> and *n*-Bu<sub>4</sub>NClO<sub>4</sub>.

energy change of electron transfer ΔG<sup>o</sup><sub>et</sub> by using Marcus equation (eq 10)<sup>43</sup> equal to the activation Gibbs energy when ΔG<sup>o</sup><sub>et</sub> = 0.

$$\Delta G_{et}^* = \Delta G_0^* \left( 1 + \frac{\Delta G_{et}^o}{4\Delta G_0^*} \right)^2 \quad (10)$$

Then, the transfer coefficient β is given as the function of ΔG<sup>o</sup><sub>et</sub> by differentiating eq 10 with respect to ΔG<sup>o</sup><sub>et</sub> (eq 11). From eq

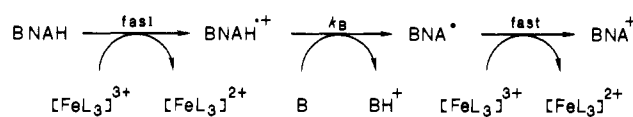
$$\beta = \frac{1}{2} + \frac{1}{8} \frac{\Delta G_{et}^o}{\Delta G_0^*} \quad (11)$$

11 are derived relations of oxidation and reduction peak potentials with the standard oxidation and reduction potentials when ΔG<sup>o</sup><sub>et</sub> = E°(PyH<sub>2</sub><sup>•+</sup>/PyH<sub>2</sub>) - E<sup>p</sup>(PyH<sub>2</sub><sup>•+</sup>/PyH<sub>2</sub>) (eq 12) and ΔG<sup>o</sup><sub>et</sub> = E<sup>p</sup>(PyH<sup>•+</sup>/PyH<sup>+</sup>) - E°(PyH<sup>•+</sup>/PyH<sup>+</sup>) (eq 13), respectively.

$$E^p(\text{PyH}_2^{\bullet+}/\text{PyH}_2) = E^\circ(\text{PyH}_2^{\bullet+}/\text{PyH}_2) + 4(1 - 2\beta)\Delta G_0^* \quad (12)$$

$$E^p(\text{PyH}^{\bullet+}/\text{PyH}^+) = E^\circ(\text{PyH}^{\bullet+}/\text{PyH}^+) - 4(1 - 2\beta)\Delta G_0^* \quad (13)$$

The E<sup>p</sup>(PyH<sub>2</sub><sup>•+</sup>/PyH<sub>2</sub>) and E<sup>p</sup>(PyH<sup>•+</sup>/PyH<sup>+</sup>) values at various sweep rates are plotted against 4(1 - 2β) in which the β values are obtained from the width of the wave E<sup>p</sup> - E<sup>p/2</sup> by using eq 9. Typical examples of the plots E<sup>p</sup>(PyH<sub>2</sub><sup>•+</sup>/PyH<sub>2</sub>) and E<sup>p</sup>(PyH<sup>•+</sup>/PyH<sup>+</sup>) vs. 4(1 - 2β) are shown in Figure 3 (parts a and b, respectively) where the observed linear correlations agree well with eq 12 and 13. Thus, from the intercepts of the linear plots, the E°(PyH<sub>2</sub><sup>•+</sup>/PyH<sub>2</sub>) and E°(PyH<sup>•+</sup>/PyH<sup>+</sup>) values are determined as listed in Table III, which shows that the one-electron oxidation potential of X-BNAH is shifted to the positive direction with decreasing the donor ability of the substituent X. The one-electron oxidation potentials of various NADH model compounds in MeCN (0.50–0.80 V) are similar to that of NADH in H<sub>2</sub>O reported by Miller et al.<sup>44</sup> (0.69 V),<sup>45</sup> while the one-electron reduction potentials of X-BNA<sup>•+</sup> (-1.1 V) are more negative than that of NAD<sup>•+</sup> (-0.70 V).<sup>45,46</sup> An important point to note from Table III is that the one-electron reduction potential of AcH<sup>•+</sup> (-0.43 V) is much more positive than those of X-BNA<sup>•+</sup> (-1.1 V) while the one-electron oxidation potential of AcH<sub>2</sub> (0.80 V) is only

**Scheme I****Table IV.** Rate Constants k<sub>B</sub> for the Deprotonation of the Radical Cations of PyH<sub>2</sub> by Pyridine Derivatives in MeCN at 298 K and the pK<sub>a</sub> Values of Pyridine Derivatives

pyridine derivative	pK <sub>a</sub> <sup>a</sup>	log k <sub>B</sub> (M <sup>-1</sup> s <sup>-1</sup> )			
		BNAH <sup>a</sup>	4-CIBNAH	2,4-Cl <sub>2</sub> BNAH	AcH <sub>2</sub>
3,5-dichloropyridine	0.67	3.2	4.0	3.8	4.9
3-cyanopyridine	1.45	3.8	4.4	4.4	5.4
4-cyanopyridine	1.86	4.1	5.0	4.8	6.0
3-bromopyridine	2.84	5.0	5.7	5.5	6.2
3-acetylpyridine	3.18	5.4	5.9	5.7	6.1
4-acetylpyridine	3.51	5.6	6.1	5.8	6.2
pyridine	5.29	6.0	6.2	5.9	6.3
2-aminopyridine	6.82	6.1			

<sup>a</sup> Taken from ref 17a.

**Table V.** pK<sub>a</sub> Values of Radical Cations of NADH Model Compounds

NADH model compd	pK <sub>a</sub>
BNAH <sup>a</sup>	3.6
4-CIBNAH	3.4
2,4-Cl <sub>2</sub> BNAH	3.3
AcH <sub>2</sub>	2.0

<sup>a</sup> Taken from ref 17a.

slightly more positive than those of X-BNAH (0.50–0.67 V). Such a positive shift of the reduction potential of AcH<sup>•+</sup> relative to X-BNA<sup>•+</sup> may be ascribed to the delocalization of the unpaired electron of AcH<sup>•+</sup>. A similar one-electron reduction potential has been reported in the case of *N*-methyl-9-phenyl-acridinium ion (-0.46 V) which shows a reversible cyclic voltammogram.<sup>47</sup> It should also be noted that the one-electron oxidation potential of X-BNAH in the presence of Mg<sup>2+</sup> (5.0 × 10<sup>-2</sup> M) in MeCN is shifted to the positive direction (ca. +0.2 V) relative to that in its absence by forming the complex with Mg<sup>2+</sup> ion (eq 4) and shows no further shift in the presence of much more concentrated Mg<sup>2+</sup> ion (1.6 M),<sup>21</sup> while that of AcH<sub>2</sub> which has no carbonyl group to interact with Mg<sup>2+</sup> ion shows essentially no shift in the presence of Mg<sup>2+</sup> ion (Table III).

**pK<sub>a</sub> Values of Radical Cations of PyH<sub>2</sub>.** The pK<sub>a</sub> value of BNAH<sup>•+</sup> has previously been determined as 3.6 from a Brønsted plot of the logarithm of the rate constant k<sub>B</sub> for the proton transfer from BNAH<sup>•+</sup> to various bases vs. pK<sub>a</sub> of the bases.<sup>17</sup> The proton-transfer rate constant k<sub>B</sub> can be determined by analyzing the kinetics of the electron-transfer reactions from BNAH to [FeL<sub>3</sub>]<sup>3+</sup> (L = 2,2'-bipyridine) in MeCN containing an excess amount of base as follows. In the presence of a base, BNAH acts as an apparent two-electron donor, when the two-electron transfer proceeds via a two-step process; first, a fast one-electron transfer from BNAH to [FeL<sub>3</sub>]<sup>3+</sup> occurs,<sup>48</sup> followed by the rate-determining deprotonation of BNAH<sup>•+</sup> by a base (B), and the subsequent second electron transfer from BNA<sup>•</sup> to [FeL<sub>3</sub>]<sup>3+</sup> is also very fast<sup>49</sup> (Scheme I). Thus, the rate of formation of [FeL<sub>3</sub>]<sup>2+</sup> for the second step of the electron-transfer reaction from BNAH

(47) Koper, N. W.; Verhoeven, J. W.; Jonker, S. A. In *Proceedings of Xth IUPAC Symposium on Photochemistry*; Presses Polytechniques Romandes: Lausanne, 1984, p 323.

(48) The Gibbs energy change of the electron transfer from BNAH to [FeL<sub>3</sub>]<sup>3+</sup> is evaluated as -11 kcal mol<sup>-1</sup> from the one-electron oxidation potential of the reductant BNAH (0.57 V in Table III) and the one-electron reduction potential of [FeL<sub>3</sub>]<sup>3+</sup> (1.06 V)<sup>39</sup> by using eq 33.

(49) The Gibbs energy change of the electron transfer from BNA<sup>•</sup> to [FeL<sub>3</sub>]<sup>3+</sup> is evaluated as -49 kcal mol<sup>-1</sup> from the one-electron oxidation potential of the reductant BNA<sup>•</sup>, which is equivalent to the one-electron reduction potential of BNA<sup>•+</sup> (-1.08 V in Table III) and the one-electron reduction potential of [FeL<sub>3</sub>]<sup>3+</sup> (1.06 V)<sup>39</sup> by using eq 33.

(43) Marcus, R. A. *J. Phys. Chem.* **1963**, *67*, 853. Marcus, R. A. *Ann. Rev. Phys. Chem.* **1964**, *15*, 155.

(44) Carlson, B. W.; Miller, L. L.; Neta, P.; Grodkowski, J. *J. Am. Chem. Soc.* **1984**, *106*, 7233.

(45) The reported potential vs. NHE is converted to that vs. SCE by subtracting 0.24 V.

(46) (a) Farrington, J. A.; Land, E. J.; Swallow, A. J. *Biochim. Biophys. Acta* **1980**, *590*, 273. (b) Anderson, R. *Ibid.* **1980**, *590*, 277.

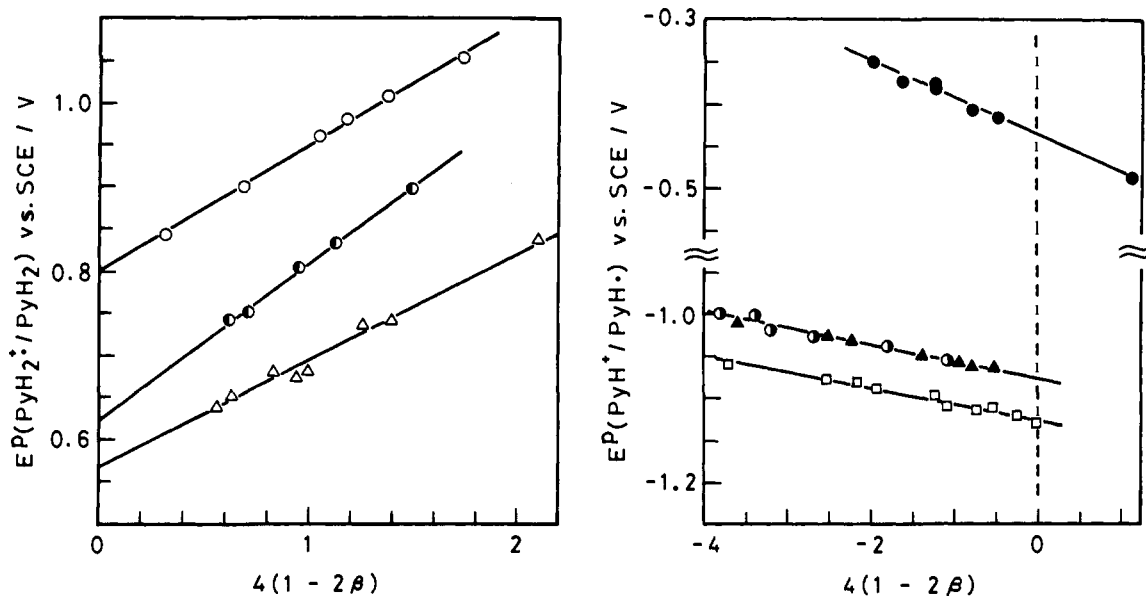


Figure 3. (a) Oxidation peak potentials of PyH<sub>2</sub>,  $E^p(\text{PyH}_2^+/\text{PyH}_2)$ , and (b) reduction peak potentials of PyH<sup>+</sup>,  $E^p(\text{PyH}^+/\text{PyH}^+)$  in MeCN at 298 K plotted as a function of transfer coefficient  $\beta$ ,  $4(1 - 2\beta)$ , see eq 12 and 13, respectively: AcH<sub>2</sub> (O), 4-CIBNAH (●), BNAH (Δ), AcH<sup>+</sup> (●), 2,4-Cl<sub>2</sub>BNA<sup>+</sup> (●), BNA<sup>+</sup> (▲), and 4-MeBNA<sup>+</sup> (□).

Table VI. Rate Constants  $k_{\text{obsd}}$  for the Hydride-Transfer Reactions from NADH Model Compounds to *p*-Benzoquinone Derivatives (Q) and the One-Electron Reduction Potentials of Q in the Absence and Presence of Mg<sup>2+</sup> Ion in MeCN at 298 K

<i>p</i> -benzoquinone derivative	$E^{\circ}(\text{Q}/\text{Q}^{\cdot-})$ V vs. SCE		$\log k_{\text{obsd}}^a$ (M <sup>-1</sup> s <sup>-1</sup> )											
	[Mg <sup>2+</sup> ]/M		BNAH <sup>b</sup> [Mg <sup>2+</sup> ]/M		4-MeOB- NAH [Mg <sup>2+</sup> ]/M		4- MeBNAH [Mg <sup>2+</sup> ]/M		4-CIBNAH [Mg <sup>2+</sup> ]/M		2,4- Cl <sub>2</sub> BNAH [Mg <sup>2+</sup> ]/M		AcH <sub>2</sub> [Mg <sup>2+</sup> ]/M	
	0	0.10	0	0.10	0	0.10	0	0.10	0	0.10	0	0.10	0	0.10
2,3-dichloro-5,6-dicyano- <i>p</i> -benzoquinone	0.51	0.51	6.92										6.18	6.15
2,3-dicyano- <i>p</i> -benzoquinone	0.28	0.25	5.86	4.45	6.23	4.52					5.48	3.83	4.04	4.28
<i>p</i> -chloranil	0.01	0.03	3.00	1.26	3.28	1.36	3.20				2.62	1.86	1.08	1.23
<i>p</i> -bromanil	0	-0.04	2.86	1.38	3.11	1.51	3.96	1.40	2.70		2.30	1.00	0.95	1.18
2,6-dichloro- <i>p</i> -benzoquinone	-0.18	-0.04	1.88	0.71	2.08	1.04	1.99	0.76	1.65	0.51	1.63	0.30	-0.82	-0.09
2,5-dichloro- <i>p</i> -benzoquinone	-0.18	-0.04	1.70	0.48	1.77	0.65	1.64	0.49	1.41	0.28	1.15	0.08		
chloro- <i>p</i> -benzoquinone	-0.34	-0.13	0.88	0	0.69	0.15	0.76	0.08	0.36	-0.21	0.36	-0.47	-2.11	-0.92
<i>p</i> -benzoquinone	-0.50	-0.18	-1.89	-0.57										-1.80
methyl- <i>p</i> -benzoquinone	-0.58	-0.32	-2.64	-1.36										-2.36
2,6-dimethyl- <i>p</i> -benzoquinone	-0.67	-0.30	-4.08	-2.41										-3.01
trimethyl- <i>p</i> -benzoquinone	-0.75	-0.40	-4.89											-3.58

<sup>a</sup> The experimental errors of  $k_{\text{obsd}}$  are within  $\pm 5\%$ . <sup>b</sup> Taken from ref 21.

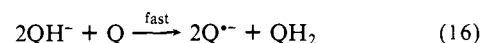
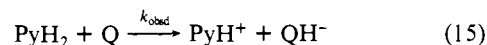
to  $[\text{FeL}_3]^{3+}$  in the presence of an excess base after the completion of the initial electron transfer is given by eq 14 where  $[\text{Fe}^{2+}]_{\infty}$

$$d[\text{Fe}^{2+}]/dt = k_B[\text{B}](\text{[Fe}^{2+}]_{\infty} - [\text{Fe}^{2+}]) \quad (14)$$

is the final concentration of  $[\text{FeL}_3]^{2+}$  which is equal to twice of the initial concentration of BNAH. The  $k_B$  values of the proton transfer from PyH<sub>2</sub><sup>+</sup> to a series of bases are listed in Table IV, together with the  $pK_a$  values of bases. Since proton transfers between normal acids and bases are known to give biphasic Brønsted plots with breaks at  $\Delta pK_a = 0$ ,<sup>50</sup> the  $pK_a$  values of PyH<sub>2</sub><sup>+</sup> can be determined from the breaks in Brønsted plots of  $\log k_B$  vs.  $pK_a$  as shown in Figure 4.<sup>51</sup> In the case of BNAH, it has been confirmed that the break of the Brønsted plot occurs at  $\Delta pK_a \cong 0$ , where the primary kinetic isotope effects show the maximum.<sup>17a</sup> The  $pK_a$  values of X-BNAH<sup>+</sup> and AcH<sub>2</sub><sup>+</sup> are listed in Table

V, which shows that the  $pK_a$  value of AcH<sub>2</sub><sup>+</sup> (2.0) is less than those of X-BNAH<sup>+</sup> (3.3–3.6).<sup>52</sup>

**Kinetics of Hydride-Transfer Reactions from PyH<sub>2</sub> to Q.** It has previously been reported that the hydride transfer from NADH model compounds to *p*-benzoquinone derivatives Q (eq 15) occurs in MeCN, followed by a subsequent fast reaction of QH<sup>-</sup> with Q to form Q<sup>•-</sup> and QH<sub>2</sub> (eq 16).<sup>20,53</sup> The rate of formation of Q<sup>•-</sup> in the presence of a large excess Q is given by eq 17,<sup>20</sup> where  $[\text{Q}^{\cdot-}]_{\infty}$  is the final concentration of Q<sup>•-</sup> which is



$$d[\text{Q}^{\cdot-}]/dt = k_{\text{obsd}}[\text{Q}](\text{[Q}^{\cdot-}]_{\infty} - [\text{Q}^{\cdot-}]) \quad (17)$$

(50) (a) Westheimer, F. H. *Chem. Rev.* **1961**, *61*, 265. (b) Bell, R. P. *The Protons in Chemistry*; Cornell: Ithaca, New York, 1973. (c) More O'Ferrall, R. A. In *Proton Transfer Reactions*; Caldin, E. F., Gold, V., Eds.; Chapman and Hall: London, 1975; Chapter 8. (d) Cohen, A. O.; Marcus, R. A. *J. Phys. Chem.* **1968**, *72*, 4249. (e) Bergman, N.-A.; Chiang, Y.; Kresge, A. J. *J. Am. Chem. Soc.* **1978**, *100*, 5954.

(51) The plateau values in Figure 4 are significantly lower than the diffusion-limited value, suggesting that there is a work term required to form the encounter complex preceding the proton transfer as is usual in a number of proton-transfer processes (see: Kresge, A. J. *Acc. Chem. Res.* **1975**, *8*, 354).

(52) The  $pK_a$  value of NADH<sup>+</sup> in H<sub>2</sub>O has been reported to be -3.5, which is significantly less than the  $pK_a$  values of PyH<sub>2</sub><sup>+</sup> in Table V, based on the thermodynamic calculation (ref 44; see, also: Martens, F. M.; Verhoeven, J. W. *Recl. Trav. Chim. Pays-Bas* **1981**, *100*, 228). However, the larger  $pK_a$  value of NADH<sup>+</sup> ( $\cong 1$ ) has recently been reported from the direct detection of NADH<sup>+</sup> by means of nanosecond laser photolysis (see: Czochralska, B.; Lindqvist, L. *Chem. Phys. Lett.* **1983**, *101*, 297).

(53) (a) Colter, A. K.; Saito, G.; Sharom, F. J. *Can. J. Chem.* **1977**, *55*, 2741. (b) Colter, A. K.; Saito, G.; Sharom, F. J.; Hong, A. P. *J. Am. Chem. Soc.* **1976**, *98*, 7833. (c) Saito, G.; Colter, A. K. *Tetrahedron Lett.* **1977**, 3325.

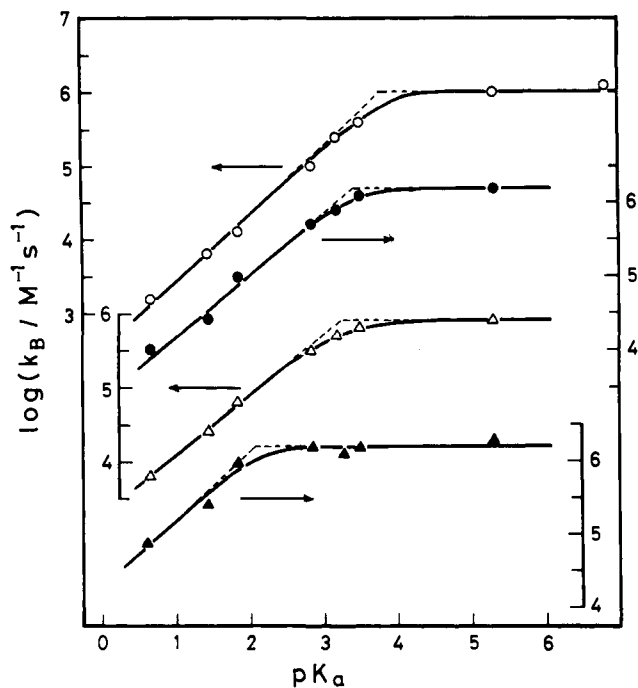


Figure 4. Brønsted plots of  $\log k_B$  for the proton-transfer reactions from the radical cations of  $\text{PyH}_2$  [BNAH (O), 4-CIBNAH (●), 2,4-Cl<sub>2</sub>BNAH (Δ), AcH<sub>2</sub> (▲)] to pyridine derivatives in MeCN at 298 K vs.  $\text{p}K_a$  of pyridine derivatives.

equal to the initial concentration of  $\text{PyH}_2$ . When  $\text{Mg}(\text{ClO}_4)_2$  was added to the  $\text{PyH}_2$ -Q system, only the hydride-transfer reaction (eq 15) occurred, and the radical anion  $\text{Q}^{\cdot-}$  has not been formed as confirmed by the electronic spectrum.<sup>21</sup> Rates of the hydride-transfer reactions from  $\text{PyH}_2$  to Q in the presence of  $\text{Mg}^{2+}$  ion in MeCN were followed by the decay of the  $\text{PyH}_2$  concentration, which is expressed by eq 18. In the case of hydride-

$$-d[\text{PyH}_2]/dt = k_{\text{obsd}}[\text{PyH}_2][\text{Q}] \quad (18)$$

transfer reactions from  $\text{AcH}_2$  to Q, the rates were followed by the formation of  $\text{AcH}^+$ . The observed rate constants  $k_{\text{obsd}}$  were determined under pseudo-first-order conditions in the presence of a large excess Q. The  $k_{\text{obsd}}$  values in the absence and presence of 0.10 M  $\text{Mg}^{2+}$  ion are summarized in Table VI, together with the one-electron reduction potentials of Q in the absence<sup>20</sup> and presence of 0.10 M  $\text{Mg}^{2+}$  ion in MeCN.<sup>21</sup> It is shown in Table VI that the rate constant in the absence of  $\text{Mg}^{2+}$  ion increases with a positive shift of the reduction potential of Q  $E^\circ(\text{Q}/\text{Q}^{\cdot-})$ , spanning a range of more than  $10^{11}$ , and the rate constant with the same quinone decreases in the order 4-MeOBNAH > 4-MeBNAH > BNAH > 4-CIBNAH > 2,4-Cl<sub>2</sub>BNAH > AcH<sub>2</sub> in accordance with an increase of the  $E^\circ(\text{PyH}_2^{\cdot+}/\text{PyH}_2)$  value (Table VI).

## Discussion

**Gibbs Energy Changes of Electron, Proton, Hydrogen, and Hydride Transfers.** On the basis of the results in the present study, we can now evaluate the Gibbs energy change of each step of the hydride-transfer reaction from  $\text{PyH}_2$  to Q, i.e., that of the initial electron transfer from  $\text{PyH}_2$  to Q ( $\Delta G^\circ_{\text{et}}$ ), the subsequent proton transfer from  $\text{PyH}_2^{\cdot+}$  to  $\text{Q}^{\cdot-}$  ( $\Delta G^\circ_{\text{H}^+}$ ), and the second electron transfer from  $\text{PyH}^+$  to  $\text{QH}^+$  ( $\Delta G^\circ_{\text{et}}$ ) as well as the Gibbs energy change of the hydrogen transfer from  $\text{PyH}_2$  to Q ( $\Delta G^\circ_{\text{H}}$ ) and that of the overall transfer of a hydride ion from  $\text{PyH}_2$  to Q ( $\Delta G^\circ_{\text{H}^-}$ ) as follows. The  $\Delta G^\circ_{\text{et}}$  values are obtained from the one-electron redox potentials of  $\text{PyH}_2$   $E^\circ(\text{PyH}_2^{\cdot+}/\text{PyH}_2)$  and Q  $E^\circ(\text{Q}/\text{Q}^{\cdot-})$  by using eq 19

$$\Delta G^\circ_{\text{et}}/F = E^\circ(\text{PyH}_2^{\cdot+}/\text{PyH}_2) - E^\circ(\text{Q}/\text{Q}^{\cdot-}) \quad (19)$$

The  $E^\circ(\text{PyH}_2^{\cdot+}/\text{PyH}_2)$  and  $E^\circ(\text{Q}/\text{Q}^{\cdot-})$  values are given in Table III and VI, respectively. The  $\Delta G^\circ_{\text{et}}$  values are also obtained from

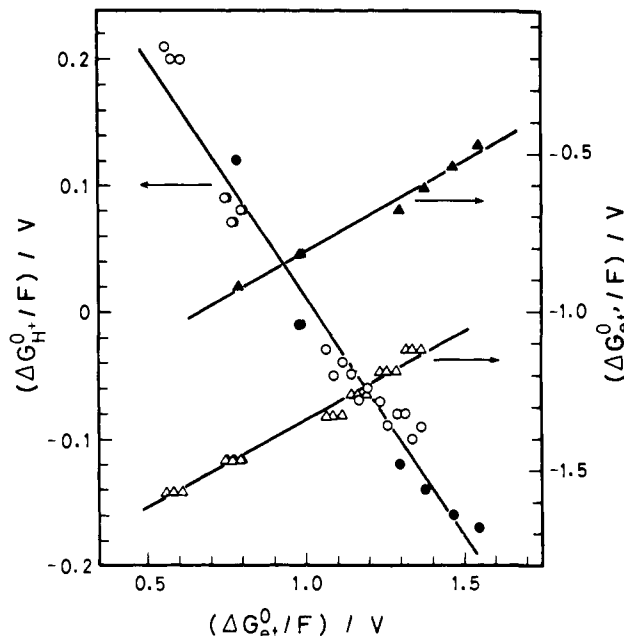


Figure 5. Correlations of the Gibbs energy changes of the proton-transfer reactions from X-BNAH<sup>+</sup> (O) and AcH<sub>2</sub><sup>+</sup> (●) to Q<sup>·-</sup> ( $\Delta G^\circ_{\text{H}^+}$ ) and the electron-transfer reactions from X-BNA<sup>+</sup> (Δ) and AcH<sup>+</sup> (▲) to QH<sup>+</sup> ( $\Delta G^\circ_{\text{et}}$ ) with the Gibbs energy change of the electron-transfer reactions from X-BNAH and AcH<sub>2</sub> to Q ( $\Delta G^\circ_{\text{et}}$ ).

the one-electron redox potentials of  $\text{PyH}^+$   $E^\circ(\text{PyH}^+/\text{PyH}^{\cdot+})$  and  $\text{QH}^+$   $E^\circ(\text{QH}^+/\text{QH}^{\cdot+})$  by using eq 20 where the  $E^\circ(\text{PyH}^+/\text{PyH}^{\cdot+})$

$$\Delta G^\circ_{\text{et}}/F = E^\circ(\text{PyH}^+/\text{PyH}^{\cdot+}) - E^\circ(\text{QH}^+/\text{QH}^{\cdot+}) \quad (20)$$

values are also given in Table III, and the  $E^\circ(\text{QH}^+/\text{QH}^{\cdot+})$  values of various *p*-benzoquinone derivatives have been reported by Rich et al.<sup>25a</sup> On the other hand, the  $\Delta G^\circ_{\text{H}^+}$  values can be determined from the  $\text{p}K_a$  values of  $\text{PyH}_2^{\cdot+}$  and  $\text{QH}^+$  by using eq 21 where

$$\Delta G^\circ_{\text{H}^+} = 2.3RT[\text{p}K_a(\text{PyH}_2^{\cdot+}/\text{PyH}^{\cdot+}) - \text{p}K_a(\text{QH}^+/\text{Q}^{\cdot-})] \quad (21)$$

the  $\text{p}K_a(\text{PyH}_2^{\cdot+}/\text{PyH}^{\cdot+})$  values are listed in Table V, and the  $\text{p}K_a(\text{QH}^+/\text{Q}^{\cdot-})$  values are given in the literatures.<sup>25a</sup> It should be noted that the  $\Delta G^\circ_{\text{et}}$  and  $\Delta G^\circ_{\text{H}^+}$  values must be accepted with reservation since the reported values of  $E^\circ(\text{QH}^+/\text{QH}^{\cdot+})$ , and  $\text{p}K_a(\text{QH}^+/\text{Q}^{\cdot-})$ <sup>25a</sup> in eq 10 and 21, respectively, are those in H<sub>2</sub>O, and the use as the values in MeCN may not be correct in an absolute sense because of the different solvation between H<sub>2</sub>O and MeCN.<sup>54</sup> However, these values can be safely used for comparison between different NADH model compounds (X-BNAH and AcH<sub>2</sub>), which is the main theme of this study.<sup>55</sup>

By using these values obtained by eq 19–21, the correlations of  $\Delta G^\circ_{\text{et}}$  with  $\Delta G^\circ_{\text{H}^+}$  and  $\Delta G^\circ_{\text{et}}$  are obtained as shown in Figure 5.<sup>56</sup> It can be seen that there is a single linear correlation between  $\Delta G^\circ_{\text{H}^+}$  and  $\Delta G^\circ_{\text{et}}$  for both X-BNAH (open circles) and AcH<sub>2</sub> (closed circles) as expressed by eq 22 but that there are two

$$\Delta G^\circ_{\text{H}^+} = 0.39F - 0.37\Delta G^\circ_{\text{et}} \quad (\text{for both X-BNAH and AcH}_2) \quad (22)$$

separate linear correlations between  $\Delta G^\circ_{\text{et}}$  and  $\Delta G^\circ_{\text{et}}$  for X-

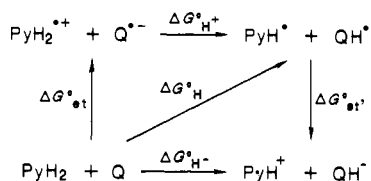
(54) However, the sensitivity of  $E^\circ(\text{Q}/\text{Q}^{\cdot-})$  to substituent effects is approximately independent of solvents (H<sub>2</sub>O and MeCN); for methyl-substituted *p*-benzoquinone derivatives,  $E^\circ(\text{Q}/\text{Q}^{\cdot-})$  in H<sub>2</sub>O<sup>25a</sup> = 0.36 + 1.0 $E^\circ(\text{Q}/\text{Q}^{\cdot-})$  in MeCN,<sup>20a</sup> where the correlation coefficient is 0.999.

(55) Both the one-electron oxidation potentials of X-BNAH and AcH<sub>2</sub> as well as the one-electron reduction potentials of X-BNA<sup>+</sup> and AcH<sup>+</sup> have been determined in the same solvent (i.e., MeCN, see Table III).

(56) The plots in Figure 5 include the data of  $\text{PyH}_2$  (BNAH, 4-CIBNAH, 2,4-Cl<sub>2</sub>BNAH, AcH<sub>2</sub>) for which all the values of  $E^\circ(\text{PyH}_2^{\cdot+}/\text{PyH}_2)$ ,  $E^\circ(\text{PyH}^+/\text{PyH}^{\cdot+})$ , and  $\text{p}K_a(\text{PyH}_2^{\cdot+}/\text{PyH}^{\cdot+})$  have been determined in this study and those Q (*p*-chloranil, 2,6-dichloro-*p*-benzoquinone, 2,5-dichloro-*p*-benzoquinone, *p*-benzoquinone, methyl-*p*-benzoquinone, 2,6-dimethyl-*p*-benzoquinone, trimethyl-*p*-benzoquinone) for which all the values of  $E^\circ(\text{Q}/\text{Q}^{\cdot-})$ ,  $E^\circ(\text{QH}^+/\text{QH}^{\cdot+})$ , and  $\text{p}K_a(\text{QH}^+/\text{Q}^{\cdot-})$  are known.



## Scheme II



BNAH (open triangles) and AcH<sub>2</sub> (closed triangles) as expressed by eq 23 and 24, respectively. Such different intercepts between

$$\Delta G_{\text{et}}^{\circ} = -1.91F + 0.56\Delta G_{\text{et}}^{\circ} \quad (\text{for X-BNAH}) \quad (23)$$

$$\Delta G_{\text{et}}^{\circ} = -1.38F + 0.57\Delta G_{\text{et}}^{\circ} \quad (\text{for AcH}_2) \quad (24)$$

X-BNAH and AcH<sub>2</sub> with the same slope (eq 23 and 24) are ascribed to the large difference in the one-electron reduction potentials between X-BNA<sup>+</sup> (-1.08 V) and AcH<sup>+</sup> (-0.43 V).

The relationship of  $\Delta G_{\text{H}}^{\circ}$  and  $\Delta G_{\text{H}^+}^{\circ}$  with  $\Delta G_{\text{et}}^{\circ}$ ,  $\Delta G_{\text{H}}^{\circ}$ , and  $\Delta G_{\text{et}}^{\circ}$  is shown in Scheme II. It is readily recognized that  $\Delta G_{\text{H}}^{\circ}$  and  $\Delta G_{\text{H}^+}^{\circ}$  are given by eq 25 and 26, respectively. Thus, by

$$\Delta G_{\text{H}}^{\circ} = \Delta G_{\text{et}}^{\circ} + \Delta G_{\text{H}^+}^{\circ} \quad (25)$$

$$\Delta G_{\text{H}^+}^{\circ} = \Delta G_{\text{et}}^{\circ} + \Delta G_{\text{H}^+}^{\circ} + \Delta G_{\text{et}}^{\circ} \quad (26)$$

combining eq 22–24 with eq 25 and 26,  $\Delta G_{\text{H}}^{\circ}$  is expressed by the same linear function of  $\Delta G_{\text{et}}^{\circ}$  for both X-BNAH and AcH<sub>2</sub> while  $\Delta G_{\text{H}^+}^{\circ}$  gives two linear correlations with  $\Delta G_{\text{et}}^{\circ}$  between X-BNAH and AcH<sub>2</sub> with different intercepts albeit the slope is the same, since  $\Delta G_{\text{et}}^{\circ}$  is different between X-BNAH and AcH<sub>2</sub> owing to the large difference in the one-electron reduction potentials between X-BNA<sup>+</sup> and AcH<sup>+</sup> (Table III).

**Gibbs Energy Relationships of Hydride-Transfer Reactions.** The logarithms of rate constants for the hydride-transfer reactions from both X-BNAH and AcH<sub>2</sub> to Q in the absence of Mg<sup>2+</sup> ion in MeCN are plotted against  $\Delta G_{\text{H}^+}^{\circ}/F$  and  $\Delta G_{\text{H}}^{\circ}/F$  as shown in Figure 6 (parts a and b, respectively),<sup>57</sup> where  $\log k_{\text{obsd}}$  is expressed as two different linear functions of  $\Delta G_{\text{H}^+}^{\circ}$  between X-BNAH and AcH<sub>2</sub> (eq 27 and 28 respectively),<sup>58</sup> while  $\log k_{\text{obsd}}$  is given by the same linear function of  $\Delta G_{\text{H}}^{\circ}$  for both X-BNAH and AcH<sub>2</sub> (eq 29).<sup>58</sup> The slopes of the plots of  $\log k_{\text{obsd}}$  vs.  $\Delta G_{\text{H}^+}^{\circ}/F$  (eq 27

$$\log k_{\text{obsd}} = -3.5 - 7.9(\Delta G_{\text{H}^+}^{\circ}/F) \quad (\text{for X-BNAH}) \quad (27)$$

$$\log k_{\text{obsd}} = 0.82 - 8.5(\Delta G_{\text{H}^+}^{\circ}/F) \quad (\text{for AcH}_2) \quad (28)$$

$$\log k_{\text{obsd}} = 14.6 - 15.3(\Delta G_{\text{H}}^{\circ}/F) \quad (\text{for X-BNAH and AcH}_2) \quad (29)$$

and 28) show that as the reaction becomes more exothermic, about one-half of the change in  $\Delta G_{\text{H}^+}^{\circ}$  is reflected in the activation barrier of the hydride-transfer reactions, i.e., the Brønsted slope  $\alpha = 0.5$ .<sup>59</sup> A similar Brønsted value has been reported for hydride-transfer reactions from NADH to *p*-benzoquinone and *o*-benzoquinone derivatives, being considered to support a direct hydride-transfer mechanism although it has been pointed out that a hydrogen-transfer mechanism cannot be ruled out.<sup>22</sup> However, if the intrinsic barrier of the reaction (i.e., the activation Gibbs energy when the Gibbs energy change is zero) is sufficiently large, any homologous series of reactions gives a linear Gibbs energy relationship between  $\log k_{\text{obsd}}$  and the Gibbs energy change of the reaction with  $\alpha = 0.5$ ,<sup>60</sup> providing no definitive information on the nature of the transition states. Thus, a direct hydride-transfer

(57) In the plots in Figure 6, the  $\Delta G_{\text{H}}^{\circ}$  and  $\Delta G_{\text{H}^+}^{\circ}$  values of the PyH<sub>2</sub>-Q systems, which are not included in Figure 5, are obtained by using eq 25 and 26, respectively, where the  $\Delta G_{\text{H}^+}^{\circ}$  and  $\Delta G_{\text{et}}^{\circ}$  values are estimated by using eq 22 and 23 (or 24), respectively.

(58) The linear solid lines in Figure 6 are drawn by the least-squares curve fits by using the data in the region where the linear relations of  $\Delta G_{\text{H}^+}^{\circ}$  and  $\Delta G_{\text{et}}^{\circ}$  with  $\Delta G_{\text{et}}^{\circ}$  are shown to hold (Figure 5).

(59) The slope of the plots in Figure 6a corresponds to  $-\alpha F/2.3RT$  and, therefore,  $\alpha = 8.4 \times 2.3RT/F = 0.50$ .

(60) (a) Glasstone, S.; Laidler, K. J.; Eyring, H. *The Theory of Rate Processes*; McGraw Hill: New York, 1941; p 145. (b) Levine, R. D. *J. Phys. Chem.* **1979**, *83*, 159.

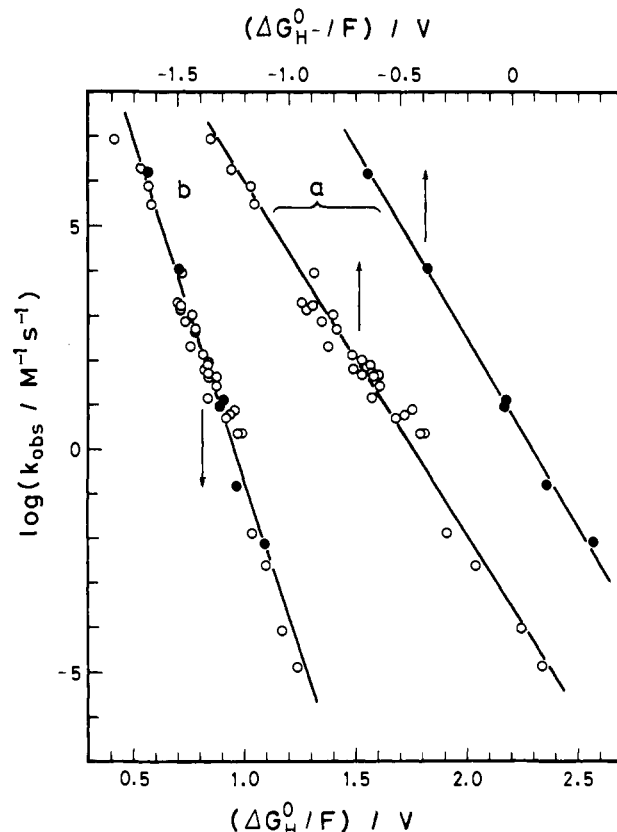


Figure 6. Plots of  $\log k_{\text{obsd}}$  for the hydride-transfer reactions from PyH<sub>2</sub> [X-BNAH (O) and AcH<sub>2</sub> (●)] to Q in MeCN at 298 K vs. (a) the Gibbs energy change of the hydride-transfer reactions from PyH<sub>2</sub> to Q ( $\Delta G_{\text{H}}^{\circ}/F$ ) and (b) the Gibbs energy change of the hydrogen-transfer reactions from PyH<sub>2</sub> to Q ( $\Delta G_{\text{H}^+}^{\circ}/F$ ). The linear solid lines are drawn by the least-squares curve fits.<sup>59</sup>

mechanism can provide no quantitative interpretation for the different correlation of  $\log k_{\text{obsd}}$  with  $\Delta G_{\text{H}^+}^{\circ}$  between X-BNAH and AcH<sub>2</sub>.

On the other hand, the slope of *single* correlation of  $\log k_{\text{obsd}}$  with  $\Delta G_{\text{H}}^{\circ}$  (eq 29), which is about twice larger than the slopes in the plots of  $\log k_{\text{obsd}}$  vs.  $\Delta G_{\text{H}^+}^{\circ}/F$  (eq 22 and 28) indicates that the change in  $\Delta G_{\text{H}}^{\circ}$  is directly reflected in the activation barrier of the hydride-transfer reactions, i.e.,  $\alpha$  is close to unity (0.91). Thus, the *single* correlation of  $\log k_{\text{obsd}}$  with  $\Delta G_{\text{H}}^{\circ}$  for both X-BNAH and AcH<sub>2</sub>, combined with the different intercepts between X-BNAH and AcH<sub>2</sub> in the plots of  $\log k_{\text{obsd}}$  vs.  $\Delta G_{\text{H}^+}^{\circ}$  ( $= \Delta G_{\text{H}}^{\circ} + \Delta G_{\text{et}}^{\circ}$ ), reveals that the activation barrier of the hydride-transfer reactions from PyH<sub>2</sub> to Q is dependent on only  $\Delta G_{\text{H}}^{\circ}$  and thereby independent of  $\Delta G_{\text{et}}^{\circ}$ ; the different correlation of  $\log k_{\text{obsd}}$  with  $\Delta G_{\text{H}^+}^{\circ}$  between X-BNAH and AcH<sub>2</sub> is caused mainly by the difference of the reduction potentials between X-BNA<sup>+</sup> (-1.08 V) and AcH<sup>+</sup> (-0.43 V), which has no effect on the activation barrier of the overall hydride transfer.<sup>61</sup> The apparent correlation of  $\log k_{\text{obsd}}$  with  $\Delta G_{\text{H}^+}^{\circ}$  may hold only provided that  $\Delta G_{\text{et}}^{\circ}$  is correlated with  $\Delta G_{\text{H}}^{\circ}$  in a homologous series of reactions. Since  $\Delta G_{\text{H}}^{\circ}$  consists of  $\Delta G_{\text{et}}^{\circ}$  and  $\Delta G_{\text{H}^+}^{\circ}$  (eq 25), the mechanistic question is reduced to (a) a direct transfer of a hydrogen atom from PyH<sub>2</sub> to Q, followed by an exothermic electron transfer from PyH<sup>•</sup> to QH<sup>•</sup> or (b) an electron transfer from PyH<sub>2</sub> to Q in the activation process and the subsequent proton transfer from PyH<sub>2</sub><sup>•+</sup> to Q<sup>•-</sup>, followed by an exothermic electron transfer from PyH<sup>•</sup> to QH<sup>•</sup>.

(61) The differences in the  $\Delta G_{\text{H}^+}^{\circ}/F$  value between BNAH and AcH<sub>2</sub> in H<sub>2</sub>O ( $\Delta \Delta G_{\text{H}^+}^{\circ}/F$ ) has been reported to be -0.57 V (ref 11a, see, also: Ostovic, D.; Lee, I.-S. H.; Roberts, R. M. G.; Kreevoy, M. M. *J. Org. Chem.* **1985**, *50*, 4206). The  $\Delta \Delta G_{\text{H}^+}^{\circ}/F$  value in MeCN determined in this study is -0.84 V, which is more negative than the value in H<sub>2</sub>O. This difference between MeCN and H<sub>2</sub>O may be ascribed to the more positive one-electron oxidation potential of the dihydronicotinamide in H<sub>2</sub>O than that in MeCN (see ref 44).



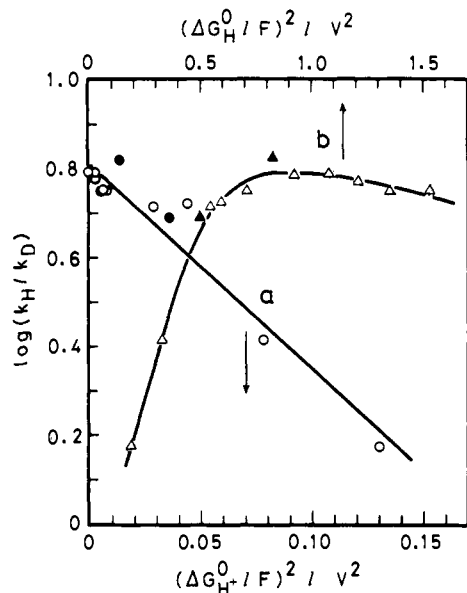


Figure 7. Plots of  $\log(k_H/k_D)$  for the hydride-transfer reactions from BNAH<sup>20</sup> and AcH<sub>2</sub><sup>53a</sup> to Q in MeCN vs. (a)  $(\Delta G^{\circ}_{H^+}/F)^2$  [BNAH (○), AcH<sub>2</sub> (●)] and (b)  $(\Delta G^{\circ}_{H^+}/F)^2$  [BNAH (Δ), AcH<sub>2</sub> (▲)], see eq 31 and 32, respectively.

**Kinetic Isotope Effects.** The kinetic isotope effects of hydride-transfer reactions from PyH<sub>2</sub> to Q may provide useful information to determine whether an actual transfer of hydrogen nucleus occurs as a form of proton or hydrogen atom. In the case of the electron-transfer activation mechanism, the observed primary kinetic isotope effects  $k_H/k_D$  may be attributed to those for the proton transfer from PyH<sub>2</sub><sup>+</sup> to Q<sup>-</sup> since no kinetic isotope effect is expected for the electron-transfer process from PyH<sub>2</sub> to Q as well as PyH<sup>+</sup> to QH<sup>\*</sup>. In such a case,  $k_H/k_D$  may be expressed as a function of the Gibbs energy change of the proton-transfer  $\Delta G^{\circ}_{H^+}$ , by using the Marcus equation (eq 30),<sup>50d,62</sup> where

$$\Delta G^{\circ}_{H^+} = \frac{\lambda_{H^+}}{4} \left( 1 + \frac{\Delta G^{\circ}_{H^+}}{\lambda_{H^+}} \right)^2 \quad (30)$$

$\lambda_{H^+}$  is the reorganization energy for the proton transfer and  $\lambda_{H^+}/4$  corresponds to the activation Gibbs energy when  $\Delta G^{\circ}_{H^+} = 0$ . From eq 30 is derived eq 31, where  $\log(k_H/k_D)_0$  is the maximum

$$\log\left(\frac{k_H}{k_D}\right) = \log\left(\frac{k_H}{k_D}\right)_0 \left( 1 - \frac{(\Delta G^{\circ}_{H^+})^2}{\lambda_{H^+}\lambda_{D^+}} \right) \quad (31)$$

kinetic isotope effect which is equal to  $(\lambda_{D^+} - \lambda_{H^+})/(4 \times 2.3RT)$ . If an actual transfer of hydrogen nucleus occurs as a form of hydrogen atom, eq 32 would be applied instead of eq 31, where  $\Delta G^{\circ}_{H^+}$ ,  $\lambda_{H^+}$ , and  $\lambda_{D^+}$  are substituted by  $\Delta G^{\circ}_{H}$ ,  $\lambda_H$ , and  $\lambda_D$ , respectively.<sup>63</sup>

$$\log\left(\frac{k_H}{k_D}\right) = \log\left(\frac{k_H}{k_D}\right)_0 \left( 1 - \frac{(\Delta G^{\circ}_H)^2}{\lambda_H\lambda_D} \right) \quad (32)$$

The reliable  $k_H/k_D$  values have been reported for the hydride-transfer reactions from BNAH<sup>20</sup> and AcH<sub>2</sub><sup>53</sup> to Q by using [4,4-D<sub>2</sub>]BNAH and [9,9-D<sub>2</sub>]AcH<sub>2</sub>, respectively, in MeCN.<sup>64</sup> The  $\log(k_H/k_D)$  values are plotted against the  $(\Delta G^{\circ}_{H^+})^2$  values as shown in Figure 7a, where  $\log(k_H/k_D)$  decreases linearly with increasing the  $(\Delta G^{\circ}_{H^+}/F)^2$  value in accordance with eq 31. From the slope and the intercept of the plot in Figure 7a, the  $\lambda_{H^+}$  and

(62) Marcus, R. A. *J. Phys. Chem.* 1968, 72, 891.

(63) The kinetic isotope effects on hydrogen-transfer reactions have been reported to show a maximum when the heat of reaction  $\Delta H$  is approximately zero and decreases with an increase in the  $|\Delta H|$  value, see: Pryor, W. A.; Kneipp, K. G. *J. Am. Chem. Soc.* 1971, 93, 5584.

(64) It has been pointed out that the  $k_H/k_D$  values determined by using [4-D<sub>1</sub>]BNAH instead of [4,4-D<sub>2</sub>]BNAH may include large experimental errors (see ref 9a).

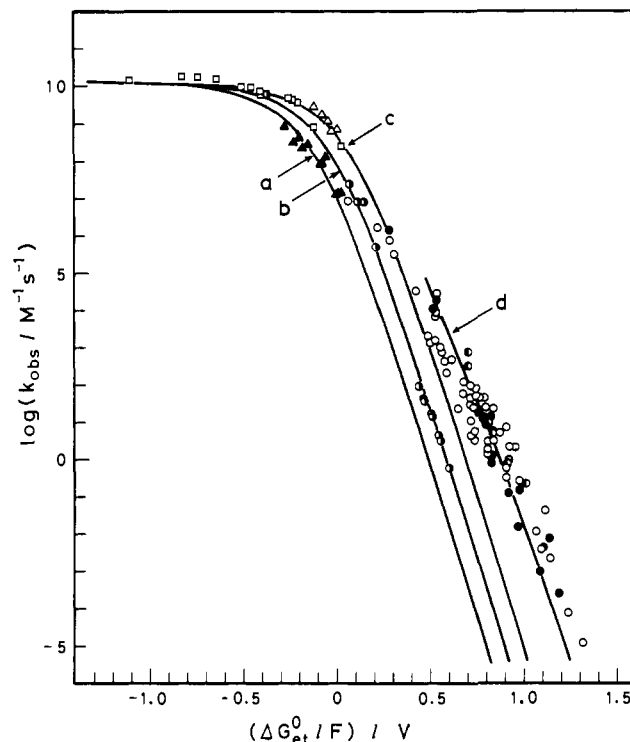


Figure 8. Plots of  $\log k_{\text{obs}}$  vs. the Gibbs energy change of the electron-transfer reactions of NADH model compounds for (a) the electron-transfer reactions from X-BNAH to [RuL<sub>3</sub>]<sup>2+</sup> in the absence and presence of Mg<sup>2+</sup> ion ( $1.0 \times 10^{-2}$  M) in MeCN (▲), (b) those from NADH to ferricenium ions<sup>44</sup> and organic monocations<sup>66</sup> in H<sub>2</sub>O (●), (c) those from X-BNAH to [RuL<sub>2</sub>L']<sup>\*</sup> in MeCN (Δ) and those from BNAH<sup>\*</sup> to organic oxidants in the absence and presence of Mg<sup>2+</sup> ion ( $5.0 \times 10^{-2}$  M) in MeCN (□), and (d) the hydride-transfer reactions from X-BNAH (○) and AcH<sub>2</sub> (●) to Q in the absence and presence of Mg<sup>2+</sup> ion (0.10 M) in MeCN at 298 K and those from NADH to Q in H<sub>2</sub>O at 303 K<sup>22</sup> (●). The solid lines in Figure 8a-c are drawn based on eq 35 by using the work terms  $w_p$  -0.10, 0, +0.10 eV, respectively, and the simulated solid line in Figure 8d is drawn based on eq 39 by using the work term -0.31 eV, see text.

$\lambda_{D^+}$  values are determined as 7.8 and 12.2 kcal mol<sup>-1</sup>, respectively. On the other hand, no linear correlation is observed between  $\log(k_H/k_D)$  and  $(\Delta G^{\circ}_H/F)^2$  as shown in Figure 7b, indicating that the primary kinetic isotope effect is not correlated with the Gibbs energy change of the hydrogen transfer  $\Delta G^{\circ}_H$ . The variation of  $k_H/k_D$  in Figure 7, which shows a sharp contrast to approximately constant  $k_H/k_D$  values (4.42–5.95) in the hydride-transfer reactions between various NADH and NAD<sup>+</sup> analogues,<sup>11b,65</sup> cannot be related to the Gibbs energy change of the overall hydride transfer  $\Delta G^{\circ}_{H^+}$ , either. Such a variation of the primary kinetic isotope effect is inconsistent with the mechanism of one-step hydride transfer since if an actual transfer of hydrogen nucleus occurs as a form of hydride ion, the constant Brønsted slope ( $\alpha = 0.5$ ) in Figure 5a (eq 27 and 28) would require the constant  $k_H/k_D$  value with the change in  $\Delta G^{\circ}_{H^+}$ . Thus, it is concluded that an actual transfer of hydrogen nucleus occurs as a form of proton and the electron-transfer activation mechanism seems to be the most plausible one to explain both the variation of the rate constants and the primary kinetic isotope effects in the hydride-transfer reactions from PyH<sub>2</sub> to Q.

In the next section, we wish to compare between the hydride-transfer and electron-transfer reactions of NADH model compounds in order to clarify the relation between them.

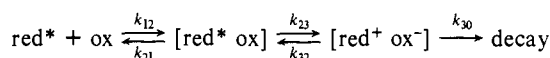
(65) Although the  $k_H/k_D$  values have been reported to be constant with the change in the equilibrium constant for the hydride-transfer reactions between NADH and NAD<sup>+</sup> analogues ( $K_H$ ) in the region  $0.70 < K_H < 2 \times 10^6$  M<sup>-1</sup> (ref 11b), the corresponding variation of  $\Delta G^{\circ}_{H^+}/F$  (-0.01 ~ 0.37 V), which is much smaller than that in this study (Figure 7), may not be wide enough to provide a definitive proof that an actual transfer of hydrogen nucleus occurs as a form of hydride ion.

**Relation between Electron-Transfer and Hydride-Transfer Reactions of NADH and Its Model Compounds.** Extensive comparison between the hydride-transfer and electron-transfer reactions of NADH and its model compounds in the absence and presence of  $Mg^{2+}$  ion is shown in Figure 8, where the logarithms of rate constants are plotted against the standard Gibbs energy change of the electron transfer  $\Delta G^\circ_{et}/F$ . Electron transfer reactions of NADH and its model compounds are classified into three groups by using differently charged oxidants (neutral, monocation, and dication); photoinduced electron-transfer reactions of X-BNAH with various neutral organic oxidants (Table II) and  $[RuL_2L']$  (Table I) in MeCN, electron-transfer reactions of NADH with organic monocations<sup>66</sup> and ferricenium cations ( $Fc^+$ )<sup>44</sup> in  $H_2O$ , and photoinduced electron-transfer reactions of X-BNAH with a dication complex  $[RuL_3]^{2+}$  in MeCN (Table I) are shown in Figure 8 (parts a, b, and c, respectively). The  $\Delta G^\circ_{et}$  values are obtained from the one-electron oxidation potentials of reductants  $E^\circ(\text{red}^+/\text{red})$  (X-BNAH in Table III, NADH,<sup>43</sup> and BNAH\*<sup>67</sup>) and the one-electron reduction potentials of oxidants  $E^\circ(\text{ox}/\text{ox}^-)$  ( $[RuL_3]^{2+}$ ,<sup>68</sup>  $[RuL_2L']^*$ ,<sup>69</sup> and organic oxidants in Table II) by using eq 33.

$$\Delta G^\circ_{et}/F = E^\circ(\text{red}^+/\text{red}) - E^\circ(\text{ox}/\text{ox}^-) \quad (33)$$

By applying the general scheme for the fluorescence quenching by an outersphere electron transfer in MeCN to the present system (Scheme III),<sup>70,71</sup> the observed rate constant  $k_{\text{obsd}}$  may be expressed

#### Scheme III



by eq 34, where  $k_{30}$  comprises all possible modes by which the

$$k_{\text{obsd}} = \frac{k_{12}}{1 + \frac{k_{21}}{k_{30}} \left( \frac{k_{30}}{k_{23}} + \frac{k_{32}}{k_{23}} \right)} \quad (34)$$

radical ion pair disappears, in particular via the back electron transfer to the ground state, being approximately equal to the frequency factor. Under such a condition, eq 34 is rewritten by eq 35,<sup>70</sup> where  $\Delta G_{23}^\ddagger$  and  $\Delta G_{23}$  are the activation Gibbs energy

$$k_{\text{obsd}} = \frac{2.0 \times 10^{10}}{1 + 0.25[\exp(\Delta G_{23}^\ddagger/RT) + \exp(\Delta G_{23}/RT)]} \quad (35)$$

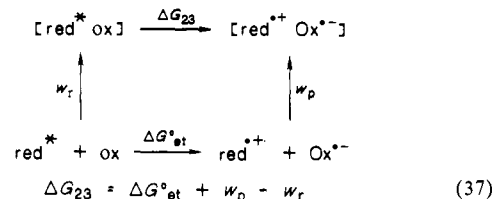
and the Gibbs energy change of the actual electron-transfer process,  $[\text{red}^* \text{ox}] \rightarrow [\text{red}^+ \text{ox}^-]$ , respectively. The relation between  $\Delta G_{23}^\ddagger$  and  $\Delta G_{23}$  is well-expressed by the Rehm-Weller equation (eq 36),<sup>70</sup> where  $\Delta G_0^\ddagger$  is the activation Gibbs energy when

$$\Delta G_{23}^\ddagger = (\Delta G_{23}/2) + [(\Delta G_{23}/2)^2 + (\Delta G_0^\ddagger)^2]^{1/2} \quad (36)$$

$\Delta G_{23} = 0$ . On the other hand, the relation between  $\Delta G_{23}$  and  $\Delta G^\circ_{et}$  is shown in Scheme IV and given by eq 37 where  $w_p$  and  $w_r$  are the work terms required to bring the products ( $\text{red}^+$  and  $\text{ox}^-$ ) and the reactants ( $\text{red}^*$  and  $\text{ox}$ ) together to the mean sep-

aration in the activated complex, which are largely coulombic, and  $w_r$  may be neglected since the reactants in the present case include neutral species. Thus, the  $k_{\text{obsd}}$  value can be calculated as a function of  $\Delta G^\circ_{et}$  by using eq 35-37.

#### Scheme IV



The calculated dependence of  $\log k_{\text{obsd}}$  on  $\Delta G^\circ_{et}$  by assuming that  $w_p = 0$  and  $\Delta G_0^\ddagger = 4.0 \text{ kcal mol}^{-1}$  agrees well with the experimental results for the electron-transfer reactions of NADH with organic monocations<sup>66</sup> and ferricenium ions ( $Fc^+$ )<sup>44</sup> as shown by the solid line in Figure 8b. Such an agreement indicates that the work term  $w_p$  is in fact negligible when the products upon the electron transfer include a neutral species such as  $Fc$ . On the other hand, when the calculated curve of  $\log k_{\text{obsd}}$  vs.  $\Delta G^\circ_{et}/F$  is shifted to  $-0.1$  and  $+0.1$  V in the abscissa, the shifted curves agree well with the experimental results for the electron-transfer reactions between X-BNAH and a dication complex  $[RuL_3]^{2+}$  and those for the reactions between neutral reactants (the BNAH\*-organic oxidant and X-BNAH- $[RuL_2L']^*$  systems) as shown by the solid lines in Figure 8 (parts a and 8c, respectively). Such agreements indicate that the  $w_p/F$  values of the radical ion pairs of the like charges (X-BNAH\* $^+$   $[RuL_3]^{2+}$ ) and the opposite charges [(BNAH\* $^+$   $\text{ox}^-$ ) and (X-BNAH\* $^+$   $[RuL_2L']^*$ )] are  $+0.1$  and  $-0.1$  eV, respectively.<sup>72</sup>

The plots in Figure 8a and c include the data in the presence of  $Mg^{2+}$  ion, which agree with the data in the absence of  $Mg^{2+}$  ion in the calculated dependence of  $\log k_{\text{obsd}}$  on  $\Delta G^\circ_{et}/F$ . Thus, the retarding effect of  $Mg^{2+}$  ion on the photoinduced electron-transfer reactions of X-BNAH (Table I and II) corresponds to the positive shift of  $\Delta G^\circ_{et}$  in the presence of  $Mg^{2+}$  ion, which is attributed to the positive shift of the one-electron oxidation potentials of the ground and excited states of X-BNAH (Table III) due to the complex formation with  $Mg^{2+}$  ion (eq 4).

In Figure 8d, the  $\log k_{\text{obsd}}$  values for the hydride transfer reactions from  $PyH_2$  (X-BNAH,  $AcH_2$ ,  $NADH^{22}$ ) to a series of *p*-benzoquinone derivatives Q in the absence and presence of  $Mg^{2+}$  ion (0.10 M) are plotted against the Gibbs energy change of the electron transfer from  $PyH_2$  to Q,  $\Delta G^\circ_{et}/F$ , which is obtained by eq 19. An important point to note in Figure 8d is that there is an approximately *single* correlation between  $\log k_{\text{obsd}}$  and  $\Delta G^\circ_{et}/F$  for different kinds of dihydropyridine compounds (X-BNAH,  $AcH_2$ , and  $NADH$  shown by the open, closed, and half-closed circles, respectively) in the absence and presence of  $Mg^{2+}$  ion, indicating that the activation barrier of the hydride-transfer reactions is well-correlated with the energetics of the electron transfer  $\Delta G^\circ_{et}$ . However, when the plot in Figure 8d is compared with the calculated dependence of  $\log k_{\text{obsd}}$  on  $\Delta G^\circ_{et}/F$  for the electron-transfer reactions of X-BNAH (the solid line in Figure 8c), the rate constants for the hydride-transfer reactions are greater than those of the electron-transfer reactions, although they become closer to each other with a decrease in  $\Delta G^\circ_{et}$ . Such a difference in the reactivity has been taken to argue against the involvement of an electron-transfer process in the hydride-transfer reactions by assuming that the work term  $w_p$  of the radical ion pair produced upon electron transfer can be neglected.<sup>22,73</sup> However, the work

(66) Grodkowski, J.; Neta, P.; Carlson, B. W.; Miller, L. L. *J. Phys. Chem.* **1983**, *87*, 3135.

(67) The one-electron oxidation potential of BNAH\* is obtained at  $-2.60$  V by subtracting the zero-zero transition energy  $\Delta E_{0,0}$  ( $= 3.17$  eV) from  $E^\circ(\text{BNAH}^+/\text{BNAH})$  ( $= 0.57$  V).<sup>38</sup>

(68) The one-electron reduction potential of  $[RuL_3]^{2+}$  has been reported to be  $0.77$  V (ref 36a).

(69) The one-electron reduction potential of  $[RuL_2L']^*$  is obtained as  $0.61$  V by adding the zero-zero transition energy  $\Delta E_{0,0}$  ( $= 2.00$  eV) to  $E^\circ([RuL_2L']/[RuL_2L']^*)$  ( $= -1.39$  V), which was determined by the cyclic voltammetry (see Experimental Section).

(70) (a) Rehm, D.; Weller, A. *Isr. J. Chem.* **1970**, *8*, 259. (b) Rehm, D.; Weller, A. *Bunsenges. Phys. Chem.* **1969**, *73*, 834.

(71) The asterisk identifies the excited state, and Scheme IV is applied to the electron-transfer reactions between BNAH\* and organic oxidants. In the case of the electron-transfer reactions between  $PyH_2$  and  $[RuL_3]^{2+}$  or  $[RuL_2L']^*$ , the asterisk should be put on ox instead of red.

(72) Similar work terms  $w_p$  for the fluorescence quenching of some aromatic acceptors by neutral donors and the luminescence quenching of  $[RuL_3]^{2+}$  by neutral donors have been reported to be  $-0.12$  and  $+0.13$  eV, respectively.<sup>38</sup>

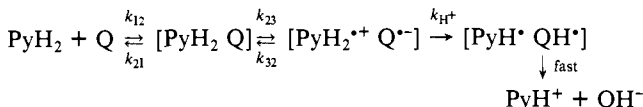
(73) Similar discussion has recently appeared in ref 23, where the redox potentials in MeCN are used to discuss the rates in  $H_2O$ . It should be pointed out, however, that the difference in  $E^\circ(Q/Q^-)$  between  $H_2O$  and MeCN (ref 54) may correspond to the difference of  $10^6$  in the rate. Thus, the discussion on the absolute values of rate constants in relation with the redox potentials must be made by using the same solvent as shown in Figure 8.

term  $w_p$  of the radical ion pair of the opposite charges produced by innersphere electron-transfer reactions via the charge-transfer (CT) complexes is expected to be much more negative than  $w_p$  in the case of outersphere electron-transfer reactions,<sup>2</sup> such as photoinduced electron-transfer reactions of X-BNAH with organic oxidants and  $[\text{RuL}_2\text{L}']$  (Figure 8c) in which the  $w_p$  value is obtained as  $-2.3 \text{ kcal mol}^{-1}$  ( $w_p/F = -0.1 \text{ eV}$ ) as described above. In fact, the  $w_p$  value of the radical ion pair for the reaction of BNAH with 2,3-dichloro-5,6-dicyano-*p*-benzoquinone has previously been evaluated as  $-7.1 \text{ kcal mol}^{-1}$  ( $w_p/F = -0.31 \text{ eV}$ ), which is much more negative than the  $w_p$  value of the outersphere electron-transfer reactions, from the formation constant of the radical ion pair ( $\log K_{\text{et}} = 4.3$ ),<sup>20</sup> by using eq 38,<sup>74</sup> where the  $E^\circ(\text{BNAH}^{+\bullet}/\text{BNAH})$  and  $E^\circ(\text{Q}/\text{Q}^{\bullet-})$  values are given in Table III and VI, respectively.

$$2.3RT \log K_{\text{et}} = F[E^\circ(\text{BNAH}^{+\bullet}/\text{BNAH}) - E^\circ(\text{Q}/\text{Q}^{\bullet-})] - w_p \quad (38)$$

In the following discussion, we wish to show that the difference in the reactivity between the electron-transfer and hydride-transfer reactions (Figure 8c and d, respectively) can be analyzed quantitatively by using the  $w_p$  value ( $-7.1 \text{ kcal mol}^{-1}$ ), based on the electron-transfer activation mechanism for the hydride-transfer reactions from  $\text{PyH}_2$  to Q (Scheme V). Scheme V is essentially

#### Scheme V



the same as Scheme III, except for the proton-transfer process ( $k_{\text{H}^+}$ ) being the route of the disappearance of the radical ion pair instead of the back electron-transfer process to the ground state ( $k_{30}$ ) in Scheme III, when the asterisk which denotes the excited state is removed from the reductant in Scheme III. Then, the observed rate constant can be expressed by eq 39 by a similar

$$k_{\text{obsd}} = \frac{2.0 \times 10^{10}}{1 + 0.25 \left[ \exp\left(\frac{\Delta G_{23}^{\ddagger}}{RT}\right) + \exp\left(\frac{\Delta G_{\text{H}^+}^{\ddagger} + \Delta G_{23}}{RT}\right) \right]} \quad (39)$$

manner to derive eq 35. The relation between  $\Delta G_{23}^{\ddagger}$  and  $\Delta G_{23}$  is given by eq 36, and  $\Delta G_{23}$  is given by eq 37, where the  $w_p$  and  $w_r$  values are taken as  $-7.1 \text{ kcal mol}^{-1}$  and 0, respectively. On the other hand,  $\Delta G_{\text{H}^+}^{\ddagger}$  is given as a function of  $\Delta G_{\text{H}^+}^\circ$  (eq 30) which can be obtained from  $\Delta G_{\text{et}}^\circ$  by eq 22. Thus, by combining together, the  $k_{\text{obsd}}$  value is calculated as a function of  $\Delta G_{\text{et}}^\circ$  by using eq 39. The calculated results are illustrated by the solid line in Figure 8d, which shows reasonable agreements with the experimental results for the hydride-transfer reactions from different kinds of dihydropyridine compounds (X-BNAH,  $\text{AcH}_2$ ,  $\text{NADH}^{22}$ ) to a series of *p*-benzoquinone derivatives Q in both the absence and presence of  $\text{Mg}^{2+}$  ion.<sup>75</sup> Such agreements strongly support the electron-transfer activation mechanism of the hydride-transfer reactions from  $\text{PyH}_2$  to Q (Scheme V).<sup>76</sup> Since the data in the absence of  $\text{Mg}^{2+}$  ion agree well with those in the presence of  $\text{Mg}^{2+}$  ion in the calculated dependence of  $\log k_{\text{obsd}}$  on  $\Delta G_{\text{et}}^\circ$ , the retarding and accelerating effects of  $\text{Mg}^{2+}$  ion on the hydride-transfer reactions depending on Q (Table VI) correspond to the shifts of  $\Delta G_{\text{et}}^\circ$  in the presence of  $\text{Mg}^{2+}$  ion, which

are attributed to the positive shifts of the one-electron oxidation potentials of X-BNAH (Table III) as well as the one-electron reduction potentials of Q due to the complex formation with  $\text{Mg}^{2+}$  ion,<sup>21</sup> according to eq 33.

#### Summary and Conclusion

The electron-transfer activation mechanism of the hydride-transfer reactions from  $\text{PyH}_2$  to Q (Scheme V) has been shown to provide a much more quantitative description of the energetic profiles of the reactions than the mechanism of a direct transfer of a hydride ion or hydrogen atom by the following reasons. (1) The  $\log k_{\text{obsd}}$  values of the hydride-transfer reactions can be expressed as the *same* function of the Gibbs energy change of the electron transfer from  $\text{PyH}_2$  to Q ( $\Delta G_{\text{et}}^\circ$ ) for both X-BNAH and  $\text{AcH}_2$  (Figure 8d), which is successfully simulated based on Scheme V, but the  $\log k_{\text{obsd}}$  values are expressed as two *different* correlations between X-BNAH and  $\text{AcH}_2$  with the Gibbs energy change of the overall hydride transfer ( $\Delta G_{\text{H}^-}^\circ$ ) (Figure 6a). (2) The variation of the primary kinetic isotope effect (Figure 7a), which can be predicted quantitatively based on Scheme V, indicated that an actual transfer of hydrogen nucleus occurs as a form of proton. Neither a direct transfer of a hydride ion nor hydrogen atom can provide a reasonable explanation on the variation of the kinetic isotope effect, which must be consistent with the variation of the rate constant. (3) The retarding and accelerating effects of  $\text{Mg}^{2+}$  ion on the hydride-transfer reactions depending on the substrate Q can be simulated quantitatively based on Scheme V (Figure 8d) by the positive shifts of the one-electron redox potentials of X-BNAH and Q, while neither mechanism of a direct transfer of a hydride ion nor hydrogen atom provides any quantitative explanation on the dual effects of  $\text{Mg}^{2+}$  ion. We have recently shown that the electron-transfer activation mechanism (Scheme V) can provide the quantitative basis also on the retarding and accelerating effects of protons on the hydride-transfer reactions from  $\text{AcH}_2$  to Q depending on Q.<sup>77</sup> (4) The difference in the reactivity between the photoinduced electron-transfer reactions and the hydride-transfer reactions via the electron-transfer activation (Scheme V) is clarified as being caused by the difference in the work term  $w_p$  required to bring the product ions to the mean separation of the activated complex between the outersphere electron-transfer and the innersphere electron-transfer reactions, respectively.<sup>76</sup>

Notwithstanding the similarities between the electron-transfer reactions (Scheme III) and the electron-transfer activation reactions (Scheme V), the difference between them must also be emphasized since the radical ion pair in Scheme V does not dissociate but disappears by the subsequent proton-transfer process, followed by the next highly exothermic electron-transfer process. Such a situation may be the main factor that has created controversies.<sup>6-19,22,23</sup> Nonetheless, the radical ion pair in Scheme V has a reality in the sense to provide a quantitative description of the energetic profile of the hydride-transfer reactions from  $\text{PyH}_2$  to Q as shown in this study. The generality of the electron-transfer activation mechanism as well as the direct detection of the radical ion pair in the endothermic region, which seems to be very difficult by the conventional methods, must be scrutinized by further studies, since the systems in this study are limited in the number owing to its strong dependence on the experimental determinations of various thermodynamic values.

**Registry No.**  $[\text{RuL}_3]^{2+}$ , 15158-62-0;  $[\text{RuL}_2\text{L}']$ , 64189-97-5; 4-Me-OBNAH, 105762-82-1; 4-MeBNAH, 19355-10-3; BNAH, 952-92-1; 4-CIBNAH, 105762-83-2; 2,4-Cl<sub>2</sub>BNAH, 105762-84-3; BCQH, 17260-79-6; 4-CIBNAH<sup>+</sup>, 105762-85-4; 2,4-Cl<sub>2</sub>BNAH<sup>+</sup>, 105762-86-5;  $\text{AcH}_2^{+\bullet}$ , 105784-79-0; 4-MeBNA<sup>+</sup>, 61777-43-3; BNA<sup>+</sup>, 15519-25-2; 4-CIBNA<sup>+</sup>, 105762-87-6; 2,4-Cl<sub>2</sub>BNA<sup>+</sup>, 105762-88-7;  $\text{AcH}^+$ , 13367-81-2; Hantzsch's ester, 1149-23-1; *N,N*-dimethylaniline, 121-69-7; *N,N*-dimethyl-*p*-toluidine, 99-97-8; *N,N'*-diphenyl-*p*-phenylenediamine, 74-31-7; diethyl fumarate, 623-91-6; diethyl terephthalate, 636-09-9; benzophenone, 119-61-9; 1-cyanonaphthalene, 86-53-3; acetophenone, 98-

(74) Equation 38 is derived from eq 19 and 37, since  $-2.3RT \log K_{\text{et}} = \Delta G_{23}^\circ$ .

(75) The calculated line (Figure 8d) is drawn in the region where the linear relations of  $\Delta G_{\text{H}^+}^\circ$  and  $\Delta G_{\text{et}}^\circ$  with  $\Delta G_{\text{et}}^\circ$  are shown to hold (Figure 5).

(76) The agreements of the calculated values with the experimental values for X-BNAH and  $\text{AcH}_2$  in MeCN as well as NADH in H<sub>2</sub>O (Figure 8) indicate also that the large work term  $w_p$  may be ascribed mainly to the strong interaction in the tight radical ion pair formed via the CT complex. Although the radical ion pair may be strongly solvated, few or no solvent molecules may be involved between the ions. This is the most important difference between outersphere and innersphere electron-transfer reactions (see ref 2a). See, also: Suppan, P. *J. Chem. Soc., Faraday Trans. 1* **1986**, 82, 509.

(77) (a) Fukuzumi, S.; Ishikawa, M.; Tanaka, T. *J. Chem. Soc., Chem. Commun.* **1985**, 1069. (b) Fukuzumi, S.; Ishikawa, M.; Tanaka, T. *Tetrahedron* **1986**, 42, 1021.

86-2; propiophenone, 93-55-0; *trans*-stilbene, 103-30-0; 4-methylacetophenone, 122-00-9; 4-methoxyacetophenone, 100-06-1; cyanobenzene, 100-47-0; methyl benzoate, 93-58-3; ethyl benzoate, 93-89-0; 3,5-dichloropyridine, 2457-47-8; 3-cyanopyridine, 100-70-9; 4-cyanopyridine, 100-48-1; 3-bromopyridine, 626-55-1; 3-acetylpyridine, 350-03-8; 4-acetylpyridine, 1122-54-9; pyridine, 110-86-1; 2-aminopyridine, 504-29-0;

2,3-dichloro-5,6-dicyano-*p*-benzene, 84-58-2; 2,3-dicyano-*p*-benzoquinone, 4622-04-2; *p*-chloranil, 118-75-2; *p*-bromanil, 488-48-2; 2,6-dichloro-*p*-benzoquinone, 697-91-6; 2,5-dichloro-*p*-benzoquinone, 615-93-0; chloro-*p*-benzoquinone, 695-99-8; *p*-benzoquinone, 106-51-4; methyl-*p*-benzoquinone, 553-97-9; 2,6-dimethyl-*p*-benzoquinone, 527-61-7; trimethyl-*p*-benzoquinone, 935-92-2; magnesium, 22537-22-0.

## Isotopic Multiplets in the Carbon-13 NMR Spectra of Aniline Derivatives and Nucleosides with Partially Deuterated Amino Groups: Effects of Intra- and Intermolecular Hydrogen Bonding

Jacques Reuben

Contribution No. 1899 from Hercules Incorporated, Research Center, Wilmington, Delaware 19894. Received June 23, 1986

**Abstract:** In aniline derivatives, the carbon-13 resonances of atoms bearing partially deuterated amino groups, as well as the resonances of vicinal carbon atoms, appear as multiplets. This phenomenon, which is due to upfield deuterium isotope effects on carbon-13 chemical shifts, is observed under conditions of slow hydrogen exchange (e.g., in Me<sub>2</sub>SO solutions). The effects are larger for groups engaged in intramolecular hydrogen bonds. Empirical expressions are presented that relate isotope effects with amino proton chemical shifts and hydrogen bond energies. Isotopic multiplets are also observed in the carbon-13 NMR spectra of partially deuterated nucleosides. The multiplet structure is altered upon formation of base pairs. These results are interpreted in terms of hydrogen exchange reactions involving uridine (or thymidine) hydrogen-bonded dimers or changes in hydrogen bond energies upon formation of guanosine-cytidine complexes. Estimates are given for the energies of individual hydrogen bonds in Watson-Crick base pairs.

The conformation, properties, and function of organic molecules in aqueous solution, including biological and synthetic polymers, depend to a large extent on the phenomenon of hydrogen bonding. Because of its fundamental importance, this phenomenon has been the subject of extensive studies by all of the available spectroscopic techniques.<sup>1</sup> Recently a correlation was observed between deuterium isotope effects on carbon-13 chemical shifts and hydrogen bond energies for phenolic and enolic hydroxyl groups engaged in intramolecular hydrogen bonds.<sup>2</sup> This paper presents results on isotopic multiplets in carbon-13 NMR spectra and deuterium isotope effects on carbon-13 chemical shifts for aniline derivatives and nucleosides. In selecting compounds for investigation, particular attention was paid to the possible presence or absence of hydrogen bonding phenomena.

Carbon atoms in the vicinity of partially deuterated functional groups containing exchangeable hydrogens exhibit multiplet structure in the proton-decoupled carbon-13 NMR spectrum. These multiplets result from small upfield deuterium isotope effects on the carbon-13 chemical shifts and are observable under conditions of slow (relative to the magnitude of the isotope effect) chemical exchange between the protio and deuterio forms.<sup>3</sup> Hydrogen ion exchange for amino groups attached to aliphatic carbons is usually fast but slows down considerably upon protonation or coordination to a metal ion. Indeed, isotopic multiplets have been observed in the carbon-13 NMR spectra of ammonium ion derivatives<sup>4</sup> and cobalt(III) complexes.<sup>5</sup> The basicities of aniline derivatives as well as of other conjugated amines are much

lower than those of aliphatic amines. Resolved proton resonances of amino and imino groups of such materials in nonhydroxylic solvents can be observed and the results of spin coupling to protons on  $\alpha$  carbons can be discerned.<sup>6</sup> Therefore, the observation of isotopic multiplets in their carbon-13 NMR spectra could be anticipated.

Intramolecular hydrogen bonding in aniline derivatives with carbonyl or nitro groups in the ortho position is a well-known phenomenon established on the basis of infrared spectral evidence.<sup>7</sup> The amino proton shifts also indicate the presence of such interactions.<sup>8</sup> Watson-Crick base pairing of nucleosides through intermolecular hydrogen bonds has been the subject of numerous investigations by NMR spectroscopy. Thus, e.g., Katz and Penman showed that formation of stable complexes between guanosine and cytidine in Me<sub>2</sub>SO solutions leads to substantial downfield shifts of the amino and imino protons.<sup>9</sup> Subsequently Newmark and Cantor obtained thermodynamic data in the same system from the concentration and temperature dependencies of the proton shifts.<sup>10</sup> More recently Petersen and Led conducted a similar investigation by carbon-13 NMR spectroscopy.<sup>11</sup> Substantial downfield shifts upon base pairing were observed for all of the base carbons, except for carbon-5 of guanosine, which shifted upfield. However, in Me<sub>2</sub>SO as the solvent no interaction between adenosine and uridine or thymidine could be detected either by proton<sup>9</sup> or carbon-13 NMR.<sup>12</sup> In order to study the

(1) Vinogradov, S. N.; Linnell, R. H. *Hydrogen Bonding*; Van Nostrand-Reinhold: New York, 1971.

(2) Reuben, J. *J. Am. Chem. Soc.* **1986**, *108*, 1735-1738.

(3) For a review see: Hansen, P. E. *Annu. Rep. NMR Spectrosc.* **1983**, *15*, 105-234.

(4) Reuben, J. *J. Am. Chem. Soc.* **1985**, *107*, 1433-1435.

(5) Yashiro, M.; Yano, S.; Yoshikawa, S. *J. Am. Chem. Soc.* **1986**, *108*, 1096-1097.

(6) Pouchert, C. J. *The Aldrich Library of NMR Spectra*; Aldrich: Milwaukee, 1983.

(7) Dyall, L. K. *Spectrochim. Acta, Part A* **1969**, *25*, 1727-1741 and references therein.

(8) Yonemoto, T.; Reynolds, W. F.; Hutton, H. M.; Schaefer, T. *Can. J. Chem.* **1965**, *43*, 2668-2677.

(9) Katz, L.; Penman, S. *J. Mol. Biol.* **1966**, *15*, 220-231.

(10) Newmark, R. A.; Cantor, C. R. *J. Am. Chem. Soc.* **1968**, *90*, 5010-5017.

(11) Petersen, S. B.; Led, J. *J. Am. Chem. Soc.* **1981**, *103*, 5308-5313.